Modelling airborne transmission of SARS-CoV-2: Risk assessment for enclosed spaces

Andre Henriques, Markus Rognlien, James Devine, Gabriella Azzopardi, Nicolas Mounet, Philip Elson, Marco Andreini, Nicola Tarocco
CERN, Geneva, Switzerland

Abstract
The global crisis triggered by the Coronavirus disease 2019 (COVID-19) pandemic has highlighted the need for a proper risk assessment of respiratory pathogens in indoor settings, due to their potential for airborne transmission. This paper is intended to document the COVID Airborne Risk Assessment (CARA) methodology, tailored for typical work spaces or public environments, enabling a quick and easy assessment of the potential exposure to SARS-CoV-2. A physical model is presented to compute the absorbed dose of virions from an exposed host, which leads to estimate the probability of contracting the disease based on the stochastic interpretation of the Wells-Riley model. The model allows for a detailed parameterization of the indoor setting, with emphasis on the effect of natural ventilation and air filtration, enabling decision makers or facility managers to perform risk assessments against airborne transmission of SARS-CoV-2. The results suggest the importance of super-emitters and superspreading events in airborne transmission: i) a small subset of infected hosts are found to emit approximately 2 orders of magnitude more viral-containing particles for any given expiratory activity and ii) loud vocalisation activities (singing or shouting) generate approximately 2 orders of magnitude more airborne particles, compared to tidal breathing. The effect of air filtration and natural ventilation suggests that i) HEPA filters significantly reduce inhaled dose of airborne viruses by a factor 5.3 in classrooms with windows closed and ii) natural ventilation strategies shall be adapted to the seasonal period since it is twice as effective during winter, compared to summer. Furthermore, the approach of a viral load threshold value was introduced, where the effect of different measures can be physically tuned such that the transmission is unlikely to occur for a given indoor setting. The properties of emerging new SARS-CoV-2 Variant of Concern (VOC) is included in the model.

Keywords
CERN report; SARS-CoV-2; COVID-19; airborne transmission; modelling; Wells-Riley; HSE.

CERN-OPEN-2021-004
15/03/2021

1 Introduction

Currently, the existing public health measures point to the importance of proper building and environmental engineering control measures, such as proper Indoor Air Quality (IAQ). This pandemic clearly raised increased awareness on airborne transmission of respiratory viruses in indoor settings. Out of the main modes of viral transmission, the airborne route of SARS-CoV-2 seems to have a significant importance to the spread of COVID-19 infections world-wide [1]. Furthermore, infection through inhaling an airborne virus could lead to more severe disease than infection from fomites [2] due to the fact that particles with smaller diameters reach deep into the lungs and bind to the cells in the alveoli [3]. The potential for presymptomatic and asymptomatic transmission is also reported, with evidence suggesting

that 30-70% of transmission happens before symptom onset [4], with viral loads peaking at around the time of symptom onset. This contrasts with other coronaviruses which peak at around 7-14 days after symptom onset [5]. The high viral loads around symptom onset suggest that SARS-CoV-2 could be easily transmissible at an early stage of infection. In occupational health and safety, the best way to ensure proper protection is to fully understand i) what are the causes of a given hazardous event and how to prevent it; ii) what are consequences arising from the hazardous event and how to protect from it. For any given risk, in order to consider the appropriate mitigation and risk control measures for our indoor spaces (e.g. workplaces, household, public spaces, transportation), a multidisciplinary risk-based approach is essential.

A physical model was developed, adapted from previous implementations of the Wells-Riley Infection approach [6, 7], to simulate the concentration of infectious viruses in an enclosed indoor volume, wherein infectious occupants with COVID-19 are shedding SARS-CoV-2 viruses. Hence, the present study only focuses on the so-called 'long-range' airborne transmission route, assuming a well-mixed box model with a homogeneous viral concentration in the entire volume. The model follows a probabilistic approach to deal with the uncertainties tied to the concerned variables such as the characteristics of this novel virus, including the properties of the emerging new Variant of Concern VOC 202012/01 [8], also called B.1.1.7 according to the Phylogenetic Assignment of Named Global Outbreak (PANGO) Lineages nomenclature system [9]. The development of such a model requires a multidisciplinary approach and understanding of the medical, mechanical and physical characteristics related to the mechanistic process of respiratory droplet nuclei emissions, the effectiveness of face covering, the dilution with outdoor air, the impact of particulate filtration, the inactivation via biological decay and dispersion models for airborne diseases in indoor environments. Human presence is the generation source of expiratory droplets and droplet nuclei (potentially containing virions), when performing vocal or pure respiratory activities [10, 11]. The droplets and droplet nuclei which are sufficiently small to be aerodynamically suspended in the air may be inhaled by the exposed occupants of the indoor setting. Particular attention is given to the winter period as a result of the low relative humidity of the ambient air, mainly due to the effect of central heating (e.g. via superheated water radiators). Low humidity air increases the evaporation of droplets and consequently the number of airborne droplet nuclei [12]. This increases the virus survival in air and reduces immune defenses of the exposed hosts [13]. The methodology presented in this paper is based on the analytical Wells-Riley approach of infectious quanta, which represent the units (i.e. *quantum*) used to quantify airborne infection [14]. To estimate the quantum generation rate, or quantum emission rate, a probabilistic approach is considered by parameterizing the viral load distributions in the respiratory tract and the volumetric concentration of droplets emitted, measured for different activities [15]. By convention, droplets and droplet nuclei will be discussed in this paper as 'airborne particles'. Once an infected occupant is emitting viruses into the volume, the physical and mechanical behavior of the floating viral-containing particles is simulated, based on the assumption of a homogeneous mixture of infectious quanta in a finite volume. With a realistic set of inputs, including a complex ventilation algorithm via open windows and flexible occupancy profile, the model allows for a combination and comparison of various mitigation measures, aimed at properly assessing the situation tailored to common practices in indoor settings. The main goal of this paper is to improve the common understanding in the modelling of airborne transmission and identify the pivotal parameters, in order to develop a quantitative action plan to help building engineers, facility managers and household individuals, in identifying which measures or combination of measures are most suitable, allowing for a tailored risk assessment and targeted investment. The results are compared with similar studies from the literature.

The model, its assumptions and the data used will be presented in Section 2. The set of possible occupation and activity profiles taken into account in the model are listed in Section 3, and simulations results in various situations follow in Section 4. Our conclusions are finally presented in Section 5.

2 Materials and Methods

2.1 Quantum of infection model

In order to quantify the concentration of a harmful agent (in this case SARS-CoV-2 virions), we need to estimate the emission source per unit time. In the 1950's, W. F. Wells introduced the notion of a quantum of infection, suggesting a hypothetical infectious dose unit for a certain pathogen [16]. A quantum, with unit q, is originally defined as the number of viable viruses suspended within one or several airborne particles, required to infect an exposed host. The original definition indicates that one quantum is equal to one infectious particle/pathogen, which would only be suitable for diseases such as tuberculosis [17]. Since typical coronaviruses seem to require more than one pathogen to initiate infection, this study includes the contribution of an equivalent quantum infectious dose qID that respects the fundamental principles introduced by Wells, i.e. one quantum represents a cluster of airborne viruses that would induce an average probability of 63% of becoming infected, if absorbed by a potential host. Thus, the number of quanta in the room represents the average infectious source strength (or infectious dose) of infectious individuals [18]. Consequently, the calculated quantum generation rate includes the combination of infectivity of the pathogen and the infectious source strength [17]. Later, a complementary study by Riley et al. [14] considered the dose of randomly distributed airborne quantum inhaled by a bystander, which would result in the increase of new infections by means of a Poisson probability distribution:

$$N = S(1 - e^{-\frac{I \cdot \mathrm{qR} \cdot p \cdot t}{Q}}), \tag{1}$$

where N is the number of new infections; S is the number of susceptible occupants exposed over time t (in h); I is the number of infectors; qR is the quantum generation rate (in $\mathrm{q\,h^{-1}}$); p the pulmonary ventilation rate (in $\mathrm{m^3\,h^{-1}}$) and Q the room ventilation rate (in $\mathrm{m^3\,h^{-1}}$).

The original exponential term of the mentioned Poisson distribution considers a constant generation rate with a homogeneous mixture and a steady-state quantum concentration, which varies with the ventilation rate. This study will cover the transient effects of the evolution of concentration over time, since a steady-state assumption is a limitation compared to the dynamics of real-world indoor outbreaks. Another limitation relates to the apparent deterministic nature of Eq. (1), which is adapted to a well-known pathogen and large populations [7]. For volume-specific risk assessments, where a small population size is foreseen, a probabilistic approach is necessary. Transmission of respiratory infections is a complex process and generally derived a posteriori from outbreaks and epidemiological data [7, 19].

Facility managers are facing a new paradigm where the need for a concrete, quick and simplified model to prevent airborne transmission in buildings and other enclosed spaces is becoming an essential part of any occupational health and safety risk assessment. According to Sze et al. [17], the alternative dose-response models for such risk assessment are more precise, as many influencing factors can be determined explicitly, allowing for fewer implicit errors in general. On the other hand, this approach requires clinical data on infectious dose to construct the dose-response curve. The Wells-Riley model allows for a quick assessment and does not require complex clinical trials with e.g. interspecies extrapolation of infectivity, and thus can be used to perform risk assessments even when the dose-response data of the pathogen is not yet available - which is the case for COVID-19 [17]. Further limitations to the use of the Wells-Riley equation are mentioned and described in this paper.

The quantum generation rate is generally estimated from epidemiological data following an outbreak investigation. In the framework of a risk management and risk prevention approach, we opted to study the projection of possible new infections before the potential outbreak takes place and predict a generation rate by relating the volumetric count of respiratory particles to the viral load of COVID-19 infected hosts [6, 15], assuming a homogeneous virus distribution in body fluids of clinical or community samples and that the number of virions in a given particle is proportional to its size. Several authors have characterized the amount of respiratory particles and their size distribution, during different vocal activities [10, 20–22]. The underlying question relates to the quantification of viable virus copies in the

substance volume of each respiratory particle, which we propose to address in Section 2.1.1.

2.1.1 Quantum generation rate (qR*)*

The quantum generation rate, qR (in q h^{-1}), is estimated by considering the volumetric rate of respiratory particles emitted by the infected host(s) and the virological characteristics. The former properties are evaluated for three different expiratory activities: i) Breathing (*index* 'b'); ii) Speaking (*index* 'sp'), iii) Shouting/Singing (*index* 'sh'). While performing the expiratory activities, the particle emissions are affected by the physical activity and loudness of the infected host's vocalisation, since the faster one breathes or the louder one speaks, the more particles per unit volume are being emitted [10, 21]. Subsequently the quantum generation rate includes the contribution of tidal volumes and amplitude of the voice. The virological characteristics include the density of viral copies per unit volume of body fluid and the virulence or infectivity. The quantum generation rate can be calculated based on the following formulation:

$$\mathrm{qR} = \frac{\mathrm{vl} \cdot E_{c,j}(D_j, c_{n,j}, f_{\mathrm{amp}}, \eta_{\mathrm{out}}) \cdot \mathrm{BR_k}}{\mathrm{qID}}, \tag{2}$$

where vl is the viral load measured from upper and lower respiratory specimens (in RNA copies per mL); $E_{c,j}$ represents the total volumetric particle emission concentration (in mL m^{-3}) over a particle size distribution D_j, for each expiratory activity j and as a function of the specific total emission concentration $c_{n,i}$ (in cm^{-3}), the vocalisation amplification factor f_{amp} (where applicable) and the outward mask efficiency η_{out} (if applicable); $\mathrm{BR_k}$ (in m^3 h^{-1}) is the breathing flow rate for a given physical activity k; qID (in RNA copies per q) is the estimated quantum infectious dose inhaled and deposited in the respiratory tract. The volume of the respiratory particles are calculated assuming each is a perfect sphere. In the present model, extending the original Wells-Riley approach where the quantum generation rate was considered constant, qR is assumed to be piecewise constant over time and follows the relationship

$$\mathrm{qR} = \begin{cases} \text{constant} > 0 & \text{when infected host is present,} \\ 0 & \text{when infected host is absent.} \end{cases}$$

Due to the large variability of the different variables discussed in this paper, a probabilistic approach is used to determine qR. The methods and variables are described in Sections 2.1.2 - 2.1.6 and summarized in Section 2.5.

2.1.2 Viral Load

For the purpose of this study, we considered data from nucleic acid amplification testing (NAAT) with a reverse-transcription polymerase chain reaction (RT-PCR) assay, to detect SARS-CoV-2 RNA copies from the respiratory tract of infected hosts. Values have a large variability, ranging from 10^2–10^{11} RNA copies per mL, covering both symptomatic, presymptomatic and asymptomatic persons [4, 23–27]. The large variability in viral load values is related to the high dynamic range over the course of the infection and would largely impact qR. This aspect is particularly relevant when the uncertainty lies on the virological conditions of the infected host during transmission. Hence, here we considered statistical distributions where the baseline descriptors correspond to the non-VOC strain(s) with respectively a mean and standard deviation of 6.6 and 1.7 (in $\log_{10}$ of RNA copies per mL). These values were determined from the available dataset of approximately 20000 RT-PCR assays, sampled from February to April 2020 [25].

In December 2020, an increasing portion of cases caused by a new variant were detected in the United Kingdom. This was considered as 'Variant Of Concern' – VOC 202012/01 (also referred to as B.1.1.7) which may significantly affect the risk of contracting SARS-CoV-2 following an exposure. There is strong evidence for the increase in the effective reproduction number of this variant, relative to

other strains of the virus [28]. The precise mechanism(s) for increased transmissibility (estimated to be in the order of 35-75% [8]) are not yet definitively understood at the time of writing. While preliminary laboratory results indicated evidence for higher viral load in infected individuals [28], it now appears that these elevated values were not substantiated by more recent studies [29]. This observation is consistent with the dynamics of cycle threshold (Ct) scores seen during rapid growth phases of the epidemic, as reported in Ref. [30]. As such, the increased infectiousness of VOC 202012/01 appears to stem from factors other than a higher viral load (cf. Section 2.1.2.1 and Section 2.1.2.2). The viral load in the respiratory fluids of infected individuals is a variable in our model, which could be adjusted to take into account increases initially observed for VOC 202012/01, if supported by sufficient scientific evidence. Note that the statistical data of viral loads are typically log-transformed.

2.1.2.1 Initial approach to VOC 202012/01 modelling

The magnitude of the increase in viral load initially observed for VOC 202012/01 was determined based on the decrease in Ct values from preliminary PCR tests analysed in [28] and [31], which were sampled in December 2020 while the epidemic of the new VOC was quickly growing. This data indicates that the median Ct score for VOC 202012/01 is reduced by a mean value of 3.8, relative to other non-VOC strains. Since the DNA is realistically multiplied by 1.9 at each cycle [31], the viral load of the variant should have been increased by a factor of $1.9^{3.8} \approx 11.5$. Our model then permits the simulation of VOC 202012/01 by applying this factor of increase to the viral load distribution. However, the resulting increase in transmission using this method significantly exceeds the reported transmission within the 35-75% range indicated in [8], hence another approach to model VOC 202012/01 shall be proposed.

2.1.2.2 Revised approach to VOC 202012/01 modelling

With the rapid evolution of studies into VOC 202012/01 early in 2021, and our observation that using higher reported viral loads did not align with expected transmission rates, we revised our initial approach. Noting that the initial data was derived from UK sampling during a highly expansionary phase of the VOC epidemic [28], and considering the established decrease in viral load with time [23,32], we interpret that the mean time between infection and test is likely to be reduced during the expansionary phase, as per Ref. [30]. This leads to an artificial increase in the observed viral load which could, theoretically, happen within any given variant (including the original one), notwithstanding the very high range of this variable. This conclusion is supported by more recent data showing no significant increase in viral load for individuals with VOC 202012/01 [29]. As a result of this insight, the baseline viral loads mentioned above (Section 2.1.2) are used independently of the variant. The data in Ref. [25] was sampled during the expansionary phase of the so-called first wave (February - April 2020), yielding larger figures compared to other phases of a given local epidemic, which fit the purpose in a risk assessment process.

Apart from the viral load, to the understanding of the authors, the other factor which could explain the increase amount of new cases of VOC 202012/01 is likely to be specific mutations enabling the virus's spike protein to bind more effectively to the ACE2 receptor (i.e. the N501Y mutation, as indicated in Ref. [33]) which could in practice impact the infectious dose qID (cf. Section 2.1.4).

2.1.3 Expiratory particle emissions

During different vocalisation activities, or by simply breathing, a large amount of particles are emitted from the mouth and/or nose, originating from the respiratory tract [3, 34]. Particles of diameter smaller than 10 µm are likely to become airborne and can remain suspended in the air for long periods of time, due to their reduced size and settling velocity [35]. Data on experimental studies measured the aerosolized particle concentration and size distribution [10, 36], although the aerosol sampling mechanisms employed, e.g. aerodynamic particle sizer (APS) or optical particle counter (OPC), are generally not capable of measuring the diameter of the respiratory droplets prior to evaporation [20]. This phenomena

can occur quasi-instantaneously after leaving the mouth or nose [37]. Understanding the initial diameter of the particle, prior to evaporation, is crucial for the quantification of the volumetric emissions [15] and consequently the quantum generation rate (qR). The particle emissions and their size distribution varies depending on the vocalisation activity. Johnson et al. [20] studied the size distributions of particle emissions for different expiratory activities and found three distinct modes associated with distinct anatomical processes in the respiratory tract: one originating from the bronchial region while breathing, another near the larynx (housing the vocal cords) which is highly active while speaking and singing; and from the oral cavity (i.e. mouth) which is active during all vocalisation. The volumetric particle emission concentration ($E_{c,j}$) is, therefore, modeled according to the aforementioned paper using a tri-modal log-normal distribution model (BLO model) [20], integrated over the particle size distribution multiplied by the volume for each diameter (assuming each particle is a perfect sphere), and within a discrete range. In the same reference, the author included an evaporation factor of 0.5 to take into account the ratio between desiccated and saturated particles. Here we propose to use an evaporation factor of 0.3, based on more recent studies [38], considering an average protein content between 3 and 76 mg per mL of nasal fluid. Since this paper is focused on airborne transmission, the limits of integration are set from 0 to 30 µm, which correspond to a desiccated particle diameter of roughly 10 µm. This assumption is reasoned knowing that particle matter above 10 µm (i.e. PM10) are most likely to settle on the floor quickly enough not to contribute to the increase of concentration in the air, with a settling time in the order of approximately 8 minutes (c.f. Section 2.2.2.3).

The particle emissions are equally affected by the amplitude of the vocalisation and this relationship is found to scale linearly with the amplitude (i.e. loudness) of the voice, while maintaining a constant size distribution [21]. An amplification factor (f_{amp}) is used to scale the emission concentration relative to 'Speaking', which is used during vocalisation. Hence, the emission concentration during 'Breathing' is not impacted by this effect since solely the Bronchial (B) mode is active.

Based on the BLO model, the volumetric particle emission concentration can be computed from

$$E_{c,j} = \int_0^{D_{\max}} \frac{1}{D} \sum_{i \in I(j)} \left[\frac{c_{n,i} \cdot f_{\mathrm{amp},j}}{\sqrt{2\pi} \cdot \sigma_{D_i}} \exp\left(-\frac{(\ln D - \mu_{D_i})^2}{2(\sigma_{D_i})^2} \right) \right] \cdot V(D) \cdot (1 - \eta_{\mathrm{out}}(D))\, dD, \quad (3)$$

where $I(j)$ is a subset of {B, L, O} determined by the expiratory activity j: for breathing $I(\mathrm{b}) = \{\mathrm{B}\}$, for speaking or shouting $I(\mathrm{sp}) = I(\mathrm{sh}) = \{\mathrm{B, L, O}\}$; $D_{\max}$ is the upper size limit of emitted particles likely to maintain airborne; μ_{D_i} and σ_{D_i} are the mean and standard deviation of the natural logarithm of the diameter for each mode (in ln µm); $c_{n,i}$ is the total particle emission concentration for each mode; $V(D)$ is the volume of the particles for a given D; $\eta_{\mathrm{out}}(D)$ is the outward mask efficiency for particles of diameter D (cf. Section 2.1.5). $E_{c,j}$ is in mL m^{-3} (i.e. volume of emitted respiratory fluid per volume of exhaled air). The amplification factor $f_{\mathrm{amp},j}$ follows [21]

$$f_{\mathrm{amp},j} = \begin{cases} 1 & \text{Breathing and Speaking,} \\ 5 & \text{Shouting.} \end{cases}$$

The geometric mean particle size in the O mode is close to 145 µm with a geometric standard deviation of 1.8 µm. This would result in a negligible impact in terms of particle emission in the range up to 30 µm, hence we conclude that the bronchial and larynx modes are the most effective for the modelling of airborne transmission. Table 1 provides the list of variables and the related distribution descriptors adopted to compute $E_{c,j}$ from Eq. (3).

2.1.4 Quantum Infectious Dose

The number of viral copies needed to cause an infection of the concerned disease defines the infectious dose of a pathogen. Such a dose depends on various factors, such as; the type of exposure (aerosol;

Table 1: Parameters of the BLO model used in the volumetric particle emission concentration in Eq. (3). The geometric mean (GM) and geometric standard deviation (GSD) of the log-normal distributions for the particle diameters are also shown. Values for $c_{n,i}$ are taken from Ref. [10] and particle diameter distribution parameters are extracted from Ref. [20], applying an evaporation correction factor of 0.3.

Tri-modal parameters for $E_{c,j}$ [a]					
Mode	$c_{n,i}$ [cm^{-3}]	μ_{D_i} [ln µm]	GM [µm]	σ_{D_i} [ln µm]	GSD [µm]
B	0.1	1.0	2.7	0.26	1.3
L	1.0	1.4	4.0	0.5	1.65
O	0.001	4.98	145	0.56	1.75

[a] Unit conversion will be necessary to compute $E_{c,j}$

intranasal; fomite) causing infection [2] or how the immune response reacts to respiratory viruses [39]. In virology, the infectious dose is normally defined using a dose-response model expressed as ID_{50} (median dose) or TCID_{50} (median tissue culture dose) that caused infection in 50% of the exposed individuals. The precise dose-response for human hosts via airborne transmission of COVID-19 is not yet determined, hence we have opted for the Wells-Riley approach estimating the quantum infectious dose (qID) as the number of viral copies that would cause a COVID-19 infection in 63% of the susceptible individuals – it can be projected as an equivalent ID_{63} [18]. Based on dose-response measurements of other known coronaviruses, e.g. SARS-CoV, the ID_{50} via airborne transmission was modeled at 280 plaque-forming units (PFU) (95% Confidence Interval (CI) from 130 to 530 PFU) [40]. Assuming a Poisson distribution, with a portion of negative samples of 50%, the conversion factor between the mean number of PFU per volume of virus stock and the quantum infections dose can be estimated as $-\ln(0.5) \approx 0.7$. Assuming the dose-response for SARS-CoV-2 also fits an exponential model, scaling from ID_{50} to TCID_{63} yields 420 PFU, which corresponds to ca. 600 infectious virions. Even lower values were found for other respiratory viruses like influenza, with an inhalation of TCID_{50} between 0.7 and 3 PFU that was enough to cause seroconversion, as well as prolonged wheezing and vomiting [41].

Based on a preliminary collection of experimental studies and modeling estimates, the median infectious dose for SARS-CoV-2 is likely to be between 10 and 1000 PFU or approximately 14 to 1400 infectious virions [42]. Nonetheless, in the absence of relevant statistical data, we have opted to use a range of three deterministic values for the probabilistic approach and compare the resulting quantum generation rates with literature: 100, 500 and 1000 RNA copies per q.

In Section 2.1.2 (and related subsections), the factor driving the increased transmissibility of VOC 202012/01 is perceived to be related to the reduction in qID. As discussed above, the absence of clear scientific evidence of qID is applicable to any SARS-CoV-2 variant, therefore, in order to find a suitable value for VOC 202012/01 we preceded by fitting qID such that the effective reproduction number with VOC 202012/01 is, on average, 55% higher compared to the original variant, assuming the same hypothetical transmission scenario [8].

The inclusion of a quantum infectious dose is necessary to normalize the generation rate so that one quantum represents the average infectious source strength with respect to the Poisson distribution in the Wells-Riley equation. Since the qID is assumed constant over time, it can be included either at this stage of the model or when calculating the quantum dose qD. The difference stage of introduction allows us to compute either the quantum concentration or the concentration of viral copies.

2.1.5 Outward effect of face covering

Face coverings are reported to be a very efficient source control measure against infection prevention and disease control [43–48]. According to the basic prevention principal of risk assessments, reducing the hazard at the source is at the top of the pyramid of mitigation measures. The so-called surgical masks are widely used and recognized as appropriate face covering devices for source control. These

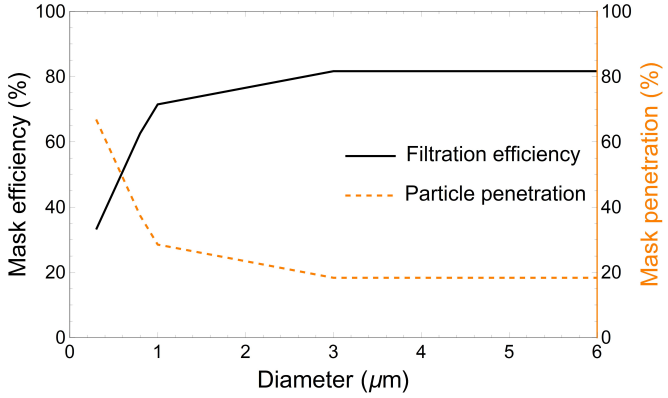

Figure 1: Effect of surgical mask in the outward direction. Black solid line represents the outward filtration efficiency of the mask, taking into account the leakages, based on empirical data; see Refs. [47, 50, 51]. The orange dashed line is the particle penetration yielding the relative fraction of particles that contribute to qR for different diameters. Note that, for D $\geq$ 3 µm, the filtration efficiency is assumed constant at 81%.

masks are manufactured following strict performance and quality requirements and are certified by the applicable national authorities. The minimum material filtration efficiency accepted in, e.g., the USA and European Union is 95 %, using the test standards ASTM F2101 and EN 14683 [49], respectively. It is important to note that these results are the filtration efficiencies of the material and do not consider the losses due to the actual positioning on the wearer's face, namely leakage. Since surgical masks are not meant to act as personal protective equipment (PPE) such as N95 or FFP2 masks, there are no requirements for leak-tightness in the test standards mentioned above. Both standards use a mean particle size of 3.0 ± 0.3 µm for the measurements, although, when breathing, the majority of the emitted particles are smaller than 3 µm [10], even when considering a saturated particle size with a geometrical mean of 2.7 µm (cf. Table 1). Reducing the particles size will have an effect on the filtration efficiency. Recent studies measured the outward filtration efficiency for surgical masks of 80% while breathing [47] and $60 - 75\%$ in the $0.7 - 2$ µm size range [50]. The result of these measurements include the effect of leaks, without performing any fit-test or fit-check procedure. The certification requirement of 95% efficiency may be used for particle sizes $\geq$ 3 µm, corrected to take into account the leakages. We assume a total leakage of 15% through the sides, nose and chin [51], which would yield an equivalent outward efficiency of 81% at sizes larger than 3 µm, comparable by the same cited measurements [47, 50]. Fig. 1 shows the values for outward efficiency (η_{out}) of surgical masks used in the model, as a function of the particle diameter.

The use of PPE (e.g. respirators), such as N95 and FFP2, are found to have a similar effect in terms of source control [47] and thus have an equivalent outward efficiency. η_{out} is equal to zero if the occupants are not wearing masks.

2.1.6 Breathing rate

A wide variation in breathing rate is observed in numerous studies. We have chosen to base our values on data originally reported by Ref. [52] as incorporated into the EPA Exposure Factors Handbook [53]. The estimation of breathing rate is critical to both the emission of infectious particles and exposure due to inhalation for an airborne pathogen. We have taken published tables from the handbook and adapted them to provide estimations of breathing rates for a variety of activities. With the available data, we have assumed an evenly distributed population from ages 16 to 61, with a male:female ratio of 1:1. Drawing on handbook values from Tables 6-17, 6-19, 6-40, 6-42, we created profiles for a number of different physical activities:

- sedentary (sitting and standing without moving),
- light intensity activity (walking, lectures, singing),

– moderate intensity activity (jogging, manual work in a laboratory or workshop),
– high intensity activity (running, exercising, heavy duty equipment manipulation, manual material transport).

The data for each activity level (Table 2) has been fitted to a log-normal distribution (cf. Fig. 2), having one distribution per activity type (incorporating the variability of the population) instead of constant values.

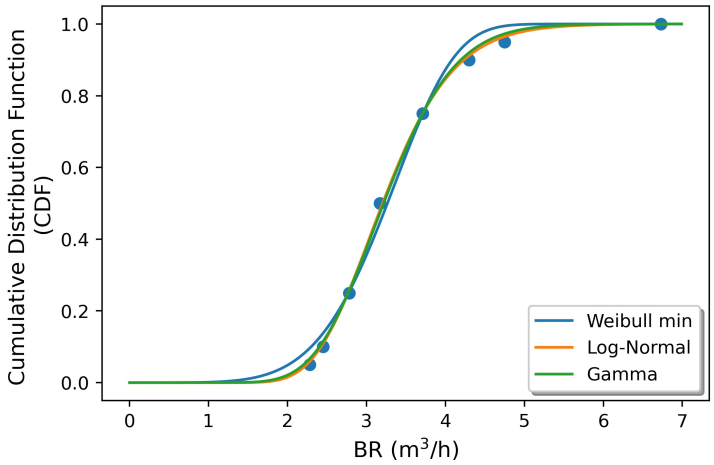

Figure 2: Outcomes of the fitting algorithm for the breathing rate distribution during a 'heavy exercise' activity, for three different kind of distribution functions, using the values from Table 2. The best fit is obtained with a Log-Normal distribution: mean (SD) of 3.28 (0.72) $m^3\ h^{-1}$.

Table 2: Statistical data on breathing rate (in $m^3\ h^{-1}$) for ages 16-61 (with equal male/female weighting).

Activity	Mean	Quantiles (%)							
		5	10	25	50	75	90	95	100
Seated	0.51	0.43	0.44	0.47	0.50	0.54	0.58	0.61	0.80
Standing	0.57	0.49	0.50	0.53	0.56	0.60	0.64	0.67	0.86
Light Exercise	1.25	1.08	1.11	1.16	1.23	1.32	1.42	1.48	1.85
Moderate Exercise	1.78	1.30	1.38	1.53	1.72	1.97	2.26	2.46	3.64
Heavy Exercise	3.30	2.28	2.45	2.78	3.17	3.71	4.30	4.75	6.73

2.2 Quantum concentration ($C(t)$)

The original Wells-Riley equation assumes a steady-state concentration. In reality, the concentration of quantum viruses depends on the dynamic effects linked to removal rates (cf. Section 2.2.2.1) and occupation profile (cf. Section 3), as well as possible changes in ventilation rate or in preventive measures (e.g. mask wearing). This study proposes a modification via a mass-balance differential equation to take into account these dynamics. Modelling the concentration of pollutants or harmful airborne agents in a room has been used extensively in the community, namely for carbon dioxide and other chemicals [54] where the pollution source generates a certain quantity of the harmful substances as a function of time. In this case, the generating source of the harmful substance is quantified by the quantum generation rate qR.

Figure 3: Simplified illustration of the infection model visualising the particle emissions of the infector via i) large size particles that fall quickly on the floor and ii) smaller size particles that spread throughout the volume with low settling velocities in typical indoors environments. The air handling unit on the top represents the renewal with clean outdoor air, the symbol on the top-right corner represents the biological decay of the virus in air and the mechanical device at the bottom represents an air cleaner with HEPA filtration grade.

2.2.1 Mass-balance model

The concentration of infectious quanta is derived from a mass balance differential equation determining the time evolution of the number of infectious quanta per unit volume, in a single-zone model:

$$\frac{dC}{dt} = \frac{\mathrm{qR} \cdot n}{V} - \lambda_{\mathrm{qRR}} \cdot C(t), \tag{4}$$

where λ_{qRR} (in h^{-1}) represents the quantum removal rate in the concerned room; V (in m^3) is the room volume; n is the number of infected hosts emitting the viruses at the same time and in equal quantities.

We assume a homogeneous dispersion of quantum particles in the room, hence potentially underestimating the infection risk for the occupants in close proximity to the infectious source [7]. This assumption implies that: 1) a proper interpersonal distance of at least $1.5 - 2$ m is ensured; 2) a single-zone ventilation mode; and 3) occupants are not in the same ventilation streamflow. These conditions (in particular the interpersonal distance) imply a slight overestimation of the risk of the long-range airborne transmission for short-term exposures, due to the time needed for the viruses to disperse and mix within the volume. The assumptions could be relieved by performing case-specific Computational Fluid Dynamics (CFD) simulations at the extra cost of a dramatic increase in complexity and computational time, thus hindering the benefits of a quick and easy risk assessment. In epidemic modeling, adopting the homogeneous mixture assumption is generally more reasonable than theoretically reconstructing the layout, airflows or interpersonal distances of the precise event where the transmission took place [17]. The integration of CFD simulations to include short-range airborne transmission and spatial viral concentration, is being considered as a potential extension of the current infection model.

Solving the differential equation, we get:

$$C(t) = \frac{\mathrm{qR} \cdot n}{\lambda_{\mathrm{qRR}} \cdot V} - \left(\frac{\mathrm{qR} \cdot n}{\lambda_{\mathrm{qRR}} \cdot V} - C_0 \right) e^{-\lambda_{\mathrm{qRR}} t}, \tag{5}$$

where $C_0 \equiv C(0)$, and the quantity $C_{\mathrm{equilibrium}} \equiv \frac{\mathrm{qR} \cdot n}{\lambda_{\mathrm{qRR}} \cdot V}$ represents the equilibrium value that is reached in the steady-state regime.

Equation (5) is valid when all variables are constant over the full time range. In our model, qR, n and λ_{qRR} may also be piecewise constant functions of time; a new value is assigned to each variable every time a condition changes in the room, in particular when an infected person(s) enters or leaves the room, or when the ventilation rates changes (which leads to a modification of λ_{qRR}, see next Section). In-between such transition times, e.g. t_n and t_{n+1}, all variables are constant and Eq. (5) is valid provided C_0 is replaced by $C(t_n)$, and t by $t - t_n$. $C(t_n)$ is in turn computed from the knowledge of the previous regime between t_{n-1} and t_n; in practice all these computations are done recursively, using an efficient caching mechanism to avoid computing the same concentration twice.

2.2.2 Quantum removal rate

The effects of air exchange, settlement or deposition inside the room, viral inactivation or biological decay and removal by filtering through an air cleaning system may be considered in a simplified form by combining the contributions from these four rates into one property λ_{qRR} [12], by means of the summation

$$\lambda_{\mathrm{qRR}} = \lambda_{\mathrm{ACH}} + \lambda_{\mathrm{dep}} + \lambda_{\mathrm{bio}} + \lambda_{\mathrm{HEPA}}, \tag{6}$$

where λ_{ACH}, λ_{dep}, λ_{bio} and λ_{HEPA} (all in h^{-1}) are the removal rates related to ventilation, gravitational settlement, biological decay and particulate filtration, respectively.

2.2.2.1 Effect of ventilation

Effective ventilation is a known preventive measure to mitigate airborne transmission [1]. The supply of clean outdoor air, referred to as 'fresh air', is important to locally dilute the airborne virus and remove the pathogens by exchanging them with fresh air.

The removal rate due to ventilation (λ_{ACH}) via mechanical or natural means, is obtained from the amount of fresh air supplied to the space and the volume of the room:

$$\lambda_{\mathrm{ACH}} = \frac{Q_{\mathrm{ACH}}}{V}, \tag{7}$$

in which Q_{ACH} represents the volumetric flow rate of fresh air supplied to the room (in $\mathrm{m}^3\,\mathrm{h}^{-1}$) and V its volume (in m^3). Q_{ACH} will depend on the type of ventilation used.

Mechanical ventilation is considered when the indoor space benefits from active means to supply fresh air, powered by equipment such as motor-driven fans and blowers normally installed in air handling units (AHU) of Heating, Ventilation and Air Conditioning (HVAC) systems. The fresh air flow rate for mechanical ventilation is considered at the level of the supply grilles or diffusers. For energy efficiency reasons, some air handling units might be suited with a mixing chamber to recycle part of the return air extracted from the indoor space. In this specific case, it is proposed to evaluate Q_{ACH} by including only the portion of fresh air supplied in the space (i.e. total supply flow of the AHU minus the recycled air flow). If the AHU is fitted with an HEPA filter, the portion of recycled air shall be included in λ_{HEPA} (cf. Section 2.2.2.4).

Although the use of mechanical systems in Europe is increasing, the overall distribution of ventilation systems allocates the greatest share to natural ventilation [55], which generates a flow of fresh air coming directly from outdoors, created by a pressure differential through permanent or temporary openings in the building's facade. This pressure differential is caused either by: i) outdoor and indoor temperature difference, where the buoyancy force arising from gravity and the difference in air densities can be used to drive the flow, or ii) wind contouring the building structure, where the velocity profile, on both facades, creates a windward and leeward exposure. To establish a wind-driven flow, the indoor

space in question shall have openings on opposite facades (windward and leeward exposure). In addition, the pressure difference depends on the mean wind boundary velocity, which fluctuates during the course of the day, ranging in intensity and geological direction. With this said, and in view of simplifying the model, this paper will only consider a buoyancy-driven flow arising from natural ventilation.

To streamline the estimation of Q_{ACH}, additional simplifications and assumptions are proposed. We consider single-sided natural ventilation, i.e. openings on one facade, although in reality occupants generally open windows and doors connecting to corridors or other volumes (i.e. cross ventilation). The later form of natural ventilation might extend the pressure gradient beyond the volume of the room yielding potentially higher flow rates that would reduce the risk, hence our choice is conservative. The limiting depth for effective single-sided ventilation is typically 5.5 m or up to 2.5 times the room height, therefore this limitation is included in the model [56].

The fresh air flow Q_{ACH} for single-sided natural ventilation is derived from a combination of Bernoulli's equation and the ideal gas law [57]:

$$Q_{\mathrm{ACH}} = \frac{C_{\mathrm{d}} \cdot A}{3} \sqrt{\frac{g \cdot h \cdot \Delta T}{T_{\mathrm{avg}}}}, \tag{8}$$

where C_{d} is the discharge coefficient; A is the area of the opening (in m^2); g is the gravitational acceleration (in $\mathrm{m\,s^{-2}}$); h is the height of the opening (in m); ΔT is the indoor/outdoor temperature difference and T_{avg} is the average indoor/outdoor air temperature (in K). Equation (8) is valid when ΔT is positive and not too large (≤ 10 K).

The discharge coefficient C_{d} represents the fraction of the opening area that is effectively used by the flow - it is smaller than the actual area of the opening because of e.g. viscous losses [57]. For sliding or side-hung windows, C_{d} is estimated at 0.6 [56, 57]. For top- or bottom- hung windows, C_{d} depends on the opening angle ϕ (in deg) and the ratio $\frac{w}{h}$ (with w the width of the window), according to the following rule [56]:

$$C_{\mathrm{d}} = C_{\mathrm{d,max}} \left[1 - \exp(-M \cdot \phi)\right], \tag{9}$$

where M and $C_{\mathrm{d,max}}$ are given for different values of $\frac{w}{h}$ in Table 3. The opening angle ϕ can be obtained via

$$\sin\left(\frac{\phi}{2}\right) = \frac{L}{2h}, \tag{10}$$

with L the size of the opening (i.e. such that $A = h \cdot L$).

For the simulation results of Section 4 we consider events in the winter period with a constant temperature difference ΔT of 10 K and in the summer with a constant ΔT of 2 K. The indoor temperature is also assumed constant during the exposure. In the absence of natural and mechanical ventilation, the removal rate λ_{ACH} will be governed by the air infiltration of typical buildings. In this study we assume a constant average value of 0.25 $\mathrm{h^{-1}}$ [58].

For this study we considered a standard sliding-type window with a height h of 1.6 m and an opening length L of 0.6 m.

Table 3: Discharge coefficient parameters for Eq. (9) for top- or bottom-hung windows, as a function of the width over height ratio $\frac{w}{h}$ [56]

	$w/h < 0.5$	$0.5 \leq w/h < 1$	$1 \leq w/h < 2$	$w/h \geq 2$
$C_{\mathrm{d,max}}$	0.612	0.589	0.563	0.548
M [$\mathrm{deg^{-1}}$]	0.06	0.048	0.04	0.038

2.2.2.2 *Biological decay*

The environmental conditions have an impact on the stability and viability of the virus in air. The half life of SARS-CoV-2 in aerosols was initially measured with a median of 1.1 hours, equivalent to SARS-CoV [59]. However, in this reference the measurements were performed at room temperature (23°C) and with a relative humidity (RH) of 65%, which is not the nominal humidity level one would assume for indoor spaces in specific seasons of the year, e.g. during the winter period. The humidity of the air in the room plays a decisive role in the capacity of the viruses to survive [60–62]. Air with a low relative humidity (typically under 40%) allows smaller particles to desiccate quickly and, while the water is completely removed, the salt content of the droplet nuclei might crystallize ending up preserving the viruses by forming a sort of protection cover. This mechanism explains why flu epidemics frequently occur during the winter period with the effect of central heating, which desiccates the air by adding sensible heat and increasing its enthalpy at a constant specific humidity. It is also apparent that the ambient humidity may play a role in the effectiveness of the bodies natural defense mechanisms against airborne viruses, with low humidity increasing susceptibility to infection.

However, a comprehensive model of the interplay between temperature, humidity and viral infectiousness remains a topic for further study. In this paper, we do not consider the effect of temperature on half life, although we acknowledge that there is significant data linking increases in temperature with a reported decrease in half life. We apply a simplification of the three-regime model proposed by Yang et al. [61] for seasonal influenza, with only two humidity regimes considered (RH < 40% and RH > 40%). In each humidity regime, we use values consistent with Figure 3A [60] for the extrapolation of the half life of the virus. In the low humidity regime (RH < 40%, 20°C), virus viability after 1 hour is 70%, compared to 20% in the high humidity regime (RH > 40%, 20°C). We use the ratio of these two values to scale the half life for the low humidity regime as follows:

- In the mid/high humidity regime, we consider a half life of 1.1, based directly on Ref. [59], such that $\lambda_{\text{bio}} = \frac{\ln(2)}{1.1} \approx 0.63\ \text{h}^{-1}$.
- In the low humidity regime, we apply the extrapolation based on the data from Ref. [61], and obtain a half life of 3.8 such that $\lambda_{\text{bio}} \approx 0.18\ \text{h}^{-1}$.

The ratio of the half lives in our low humidity and high humidity regimes is 3.5, similar to that reported in the literature, notably in Ref. [63], where median half lives of 6.4 hours (RH = 40% at 22°C) and 2.4 hours (RH = 65% at 22°C) are reported in Figure 1b, giving a ratio of 2.6. The method employed in the aforementioned study, namely capture on polypropylene surfaces, is consistent with reports of longer viral half lives. We therefore consider this to be a conservative figure for the regime RH < 40%, since the reference is taken at the start of the low humidity region.

In the model, we differentiate between the two regimes on the basis of the corresponding average seasonal indoor humidity, due to the effect of central heating. Unless specified otherwise, the default humidity regime discussed in Section 4 is RH > 40%.

2.2.2.3 *Gravitational settlement*

Once particles are airborne, they are subject to aerodynamic forces which tend to balance with the forces of gravitational nature (dead weight), with the absence of additional momentum. Using the Stokes law, one can analytically calculate the settling velocity of a certain particle, corresponding to equilibrium between the sum of the drag and buoyancy forces and the downward force due to gravity:

$$\upsilon = \frac{(\rho_{\text{p}} - \rho_{\text{air}})(D \cdot 10^{-6})^2 \cdot g}{18\ \mu_{\text{air}}}, \tag{11}$$

where, ρ_{p} and ρ_{air} (in kg m^{-3}) are the mass densities of the particle and air, respectively, g is the gravitational acceleration (in m s^{-2}), D is the diameter of the particle (in μm) and $\mu_{\text{air}} \approx 1.8 \cdot 10^{-5}$ kg m^{-1} s^{-1} (at room temperature and atmospheric pressure) is the dynamic viscosity of air.

Assuming the composition of a given airborne particle is dominated by water and/or organic solutes of similar density, the proposed mass density for ρ_{p} is 1000 kg m^{-3} [20]. The mass density of air (ρ_{air}) is taken at 1.2 kg m^{-3}. Assuming that the droplets are falling from the mouth or nose of a person standing, the height at which the terminal velocity (obtained from Eq. (11)) is reached, is considered at approximately $h = 1.5$ m. Thus, particles with a diameter $D \leq 3$ µm have a settling time higher than one hour and a half (and it even reaches more than 13 hours for $D = 1$ µm), whereas larger droplets with $D \geq 10$ µm are only able to maintain airborne for approximately 8 minutes and less (cf. Fig. 4). Therefore, the phenomenon of particle evaporation introduced in Section 2.1.3, which reduces the particles' size, has a significant effect on the total amount of airborne particles which could potentially be inhaled by exposed hosts.

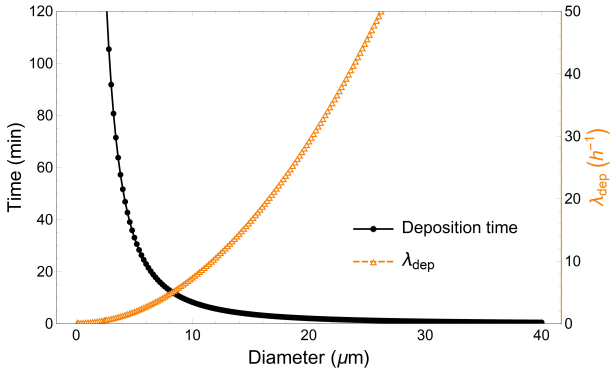

Figure 4: Effect of gravitational settling in standard indoor environments with typical air flow conditions. The solid line with circular markers represents the settling time of particles as a function of their size, assuming a terminal velocity at $h = 1.5$ m from the floor. The dashed line with the triangular markers represents the removal rate due to gravitational settling.

For simplification, we've adopted an envelope particle diameter to calculate the settling velocity. We chose it at 2.5 µm, i.e. approximately the geometric mean of the particles emitted when breathing (see Table 1) – the geometric mean, rather than arithmetic, is chosen due to the stronger effect of larger particle sizes in Eq. (3). This yields:

$$\lambda_{\mathrm{dep}} = \frac{v}{h} = 0.45\ h^{-1}, \tag{12}$$

which is in agreement with other studies [15, 19].

2.2.2.4 Air filtration

The removal of airborne particles in a closed volume can be achieved by cleaning the air using High-Efficiency Particulate Air (HEPA) fibre-based mechanical filters. HEPA filters are the most efficient mechanical filters in the submicron range, increasing the probability of capturing viral-containing droplet nuclei in the air [64,65]. The effect of this mechanism on the removal rate is determined by the volumetric flow rate of the air passing though the filter, multiplied by its efficiency (η_{f}) and taking into account the effectiveness of the system in reducing a certain percentage of the particle load within 20 minutes (PR_{20}). Figure 5 shows the effect of increasing the air exchange rate of the HEPA device on the particle removal efficiency, which can be determined by:

$$\lambda_{\mathrm{HEPA}}(\mathrm{PR}_{20}) = \frac{Q_{\mathrm{HEPA}}}{V} \cdot \eta_{\mathrm{f}}, \tag{13}$$

in which Q_{HEPA} (in m^3 h^{-1}) is the effective flow rate through the device; PR_{20} is the particle removal objective; η_{f} is the filter efficiency. For HEPA filters certified according to EN 1822 standard [66], η_{f} is 99.95 % and 99.995 %, for the corresponding H13 and H14 classes, respectively. Due to the high efficiency of both filter classes, this term can be neglected. The commercial filtering device should be

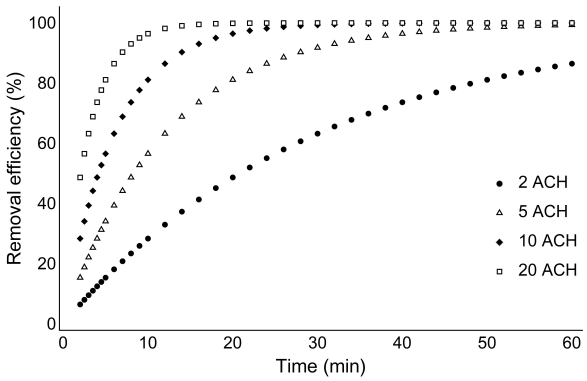

Figure 5: Time required to remove a fraction of the total particle load with HEPA filtration as a function of the mechanical performance of the device (in ACH). To reach a reasonable removal efficiency (e.g. 80 %) in an acceptable time frame (e.g. 20 min), we would need to select a device that would provide a removal rate (λ_{HEPA}) of about 5 ACH.

selected to ensure a nominal flow rate that is able to reduce sufficiently the particle load. The effectiveness of the system determines how fast the particle load is reduced in a volume. This approach is frequently used in industry, namely in the design of clean rooms [67], although this parameter is determined in the decay zone of the concentration profile ($C(t) = C_0\, e^{-\lambda_{\mathrm{qRR}}\, t}$) where the generating source is not present (i.e. $\mathrm{qR} = 0$). In reality, the effect of a constant qR > 0 in the presence of an HEPA filter will be included in the solution of Eq. (5), therefore we use the effectiveness of the filter as an input for λ_{HEPA} when selecting the device. Hence, we opted to consider a particle removal objective (PR_{20}), of at least 80% that would yield an exchange rate ≥ 5 air changes per hour (ACH). For this study we used:

$$\lambda_{\mathrm{HEPA}}(0.8) = 5\ h^{-1}, \tag{14}$$

which is comparable with other design values for biological safety labs and hospital wards [68].

2.3 Quantum dose inhaled (qD)

The dose, qD (in quantum 'q'), which is inhaled by the exposed host, is determined by integrating the quantum concentration profile over the exposure time, multiplying by the breathing flow rate, the fraction of viral-containing particles that deposit in the respiratory tract and the inward filtration efficiency of the PPE, if worn:

$$\mathrm{qD} = \int_{t1}^{t2} C(t)\ dt \cdot \mathrm{BR_k} \cdot f_{\mathrm{dep}} \cdot (1 - \eta_{\mathrm{in}}), \tag{15}$$

where t_1 and t_2 are the start and end exposure times (in h), respectively; f_{dep} is the deposition fraction in the respiratory tract and η_{in} is the inward efficiency of the PPE (values between 0 and 1).

Note that the breathing rate is directly proportional to the dose, hence the physical activity plays an important role in airborne transmission. Equation 15 is valid for a single exposure from t_1 to t_2. If during the simulated event, the susceptible hosts are exposed to multiple independent exposure scenarios (e.g. they leave the enclosed volume for a lunch break), the quantum dose rate is given by:

$$\mathrm{qD} = \sum_{i=1}^{n} \int_{t_i}^{t_{i+1}} C(t)\ dt \cdot \mathrm{BR_k} \cdot f_{\mathrm{dep}} \cdot (1 - \eta_{\mathrm{in}}), \tag{16}$$

where t_i and t_{i+1} are the start and end times (in h) of each exposure, respectively; n is the total amount of independent exposures in the same event (i.e. subject to the same quantum concentration profile).

2.3.1 Inward effect of face covering

In case the occupants are wearing PPE (e.g. respirators), such as N95 and FFP2, both the filtration efficiency and leak-tightness requirements are defined in the concerned test standards in the USA or European Union, i.e. NIOSH-42 CFR Part 84 [69] and EN 149 [70], respectively. Both standards use a mean particle size of a factor 10 smaller compared to those of surgical masks: 0.3 μm. According to EN 149, the inward leakage requirement for FFP2 is 8%. Despite knowing that source control measures, e.g. surgical masks, are not meant as PPE, they are still found to have an inward efficiency between 30% and 80% [50, 71]. This variability might be linked to how well the mask is fitted to the wearer's face. Similar to Section 2.1.5, we profit from empirical data [47, 50, 51] to derive the inward efficiency of surgical masks and use the standard certification values for PPE, which include fitting requirements. In the end the values for inward efficiency of N95/FFP2 respirators and of surgical masks are derived from:

$$\eta_{\text{in}} = \begin{cases} 0 & \text{No mask} \\ 0.50 & \text{Surgical mask} \\ 0.95 - (0.95 \cdot 0.08) = 0.87 & \text{N95/FFP2} \end{cases}$$

In the proposed model, a constant value of η_{in} is equally applied to all susceptible hosts.

2.3.2 Effect of particle deposition in respiratory tract

From a pure physical point of view, the respiratory tract acts as a filter where particle deposition is distributed along its depth [3]. Similar to a mechanical filter, the three main mechanisms are i) inertial impact: large particles (> 2.5 μm) generally deposit in the nasopharyngeal region down to the bronchi; ii) diffusion: very small particles (< 0.3 μm) diffuse and deposit randomly on the surfaces of the airways and iii) sedimentation: intermediate-size particles (between 0.3 μm and 2.5 μm) - that are small enough to go into bronchioles and alveoli but big enough to avoid the Brownian motion effect - penetrate deep into the lower respiratory tract [72]. COVID-19 infections can occur from SARS-CoV-2 virus binding to ACE receptors which are abundant in nasal and bronchial epithelium and alveolar epithelial cells, covering both upper and lower bounds of the tract [73]. Therefore, it is not prudent to consider that only the smallest particles that reach the lungs contribute to the infection. The virus can start replicating in the nose/mouth, migrating down to the airways and entering the alveolar region of the lungs to induce acute respiratory distress [74]. With this said, one can conclude that the fraction of inhaled particles that are absorbed in the respiratory tract (f_{dep}) is greater than zero, however, the respiratory tract does not absorb all the infectious aerosols which are inhaled. Even if all the particles penetrate into the pulmonary region, not all are absorbed by a susceptible host since a fraction of these particles will be re-ejected once again from the airways, while exhaling, therefore $0 < f_{\text{dep}} < 1$. A suitable practical illustration is the observation that individuals can inhale and exhale smoke particles. According to the International Commission on Radiological Protection (ICRP) particle deposition model, adapted by Hinds [72], approximately 60% of the total amount of inhaled particles are deposited in the respiratory tract, hence we use here

$$f_{\text{dep}} = 0.6\,.$$

2.4 Estimation of the Probability of Infection

The original Wells–Riley equation (Eq. (1)) predicts the number of new infections (N), based on the number of susceptible occupants (S) and, as mentioned, a Poisson probability distribution centred on the steady-state dose of quantum viruses inhaled over time (t). In this study we have included the dynamics of a transient quantum concentration over time, thus updating Eq. (1) to

$$N = S(1 - e^{-\text{qD}}), \tag{17}$$

with qD obtained from Eq. (16).

The ratio between the number of new infections and susceptible hosts corresponds to the attack rate of a certain hypothetical outbreak. This in turn leads to an estimation of the probability of infection, depending on the quantum dose, represented by

$$P(I|\mathrm{qD}) = \frac{N}{S} = (1 - e^{-\mathrm{qD}}), \tag{18}$$

where $P(I|\mathrm{qD})$ denotes the conditional probability of event I (infection) for a given value of the quantum dose qD. The probability of infection $P(I)$ can be determined as:

$$P(I) = \int_0^{+\infty} P(I|\mathrm{qD}) \cdot f(\mathrm{qD})\ d\mathrm{qD}, \tag{19}$$

in which $f(\mathrm{qD})$ represents the probability density function (PDF) of qD. The variability of the simulated quantum dose is accounted for by means of a probabilistic approach. By neglecting the effects of such a variability, $P(I)$ would be underestimated [7]. The number of new infections (N) is equivalent to the basic reproduction number (R_0), if a single individual is infected during transmission.

As mentioned above, the model predicts that each inhaled quantum of virions deposited in the respiratory tract will be considered as a potential infectious source. The original Wells–Riley formulation only predicts new cases with the assumption that the incubation period is longer than the time scale of the simulation. Since the incubation period of COVID-19 is 1-2 weeks [75], the evaluation should be within this timeframe. This assumption is acceptable since He et al. [4] found less than 0.1% of transmission to secondary cases 7 days prior to symptom onset. It is important to note that the results of infection probabilities only take into consideration the airborne transmission of the virus. It does not include short-range aerosol exposure (where the physical distance of 1-2 meters plays a critical role), nor the other known modes of SARS-CoV-2 transmission such as fomites. Hence, the results from this study are only valid when the other recommended public health & safety instructions are observed, such as adequate physical distancing, good hand hygiene and other barrier measures.

2.5 Probabilistic approach to the qR and qD estimation and infection dependency on qID and vl

In this paper, the quantum dose qD is calculated solving the integral in Eq. (16) for some given time intervals, plugging-in the concentration function from Eq. (5), where the presented variables (e.g. f_{dep}, $\mathrm{BR_k}$, etc.) are considered as time invariant. To account for the aleatory uncertainties, which affect $\mathrm{BR_k}$, vl and qID, such variables are treated herein as random, with the result that qR, calculated by Eq. (2), is considered random as well. As mentioned in Section 2.1.6, the $\mathrm{BR_k}$ dataset [52] has been fitted with a Log-Normal distribution model. Concerning the viral load vl, despite its large variability and the fact it comes from one single source [25], the data has been considered as trustworthy. From this data, a distribution function has been obtained using the Kernel Density Estimation (KDE) technique. Table 4 summarizes the adopted distribution models and the related statistics.

Since the literature did not offer any reliable indication on the frequencies of qID (cf. Section 2.1.4), we opted to describe the randomness of qR and, therefore, qD in terms of conditional probability for a given value of qID. Thus, we refer to $f(\mathrm{qR}|\mathrm{qID})$ and $F(\mathrm{qR}|\mathrm{qID})$ respectively as the probability density function (PDF) and the cumulative distribution function (CDF) of qR for a given value qID. Analogously, for the sake of clarity, we indicate $f(\mathrm{qD}|\mathrm{qID})$ and $F(\mathrm{qD}|\mathrm{qID})$ respectively as the PDF and the CDF of qD for a given value of qID. The values of such PDFs and CDFs are estimated by applying Eqs. (2), (5) and (16) for each value $\mathrm{BR_k}$ and vl obtained by plain Monte Carlo Simulations (MCS) from the distribution models described in Table 4.

Referring to Eq. (19), the conditional probability of infection $P(I|\mathrm{qID})$ for a given value of qID can be determined as

$$P(I|\mathrm{qID}) = \int_0^{+\infty} P(I|\mathrm{qD}) \cdot f(\mathrm{qD}|\mathrm{qID})\, d\mathrm{qD}. \tag{20}$$

It is also worth to discuss qR as a function of vl and qID, as presented in Eq. (2). By plugging it in Eq. (5) and with some substitutions in Eq. (16) we may define also qD as a function of these two variables. This way, through Eq. (18) we can define the conditional probability of infection $P(I|\mathrm{vl}, \mathrm{qID})$ for given values of vl and qID. Then, Eq. (20) can be written also as $P(I|\mathrm{qID})$=$\int_0^{+\infty} P(I|\mathrm{vl}, \mathrm{qID}) \cdot f(\mathrm{vl})\, d\mathrm{vl}$, where $f(\mathrm{vl})$ is the probability density function of vl.

The results of the application of this approach are presented in the Section 4.

Table 4: Summary of random variables for qR

Random (stochastic) variables						
Expiratory Activity	Variable	Symbol	Mean	SD	Unit[a]	Fitting Distribution Model
All	Breathing flowrate	BR_k			$\mathrm{m^3\,h^{-1}}$	Log-Normal
	Seated	$\mathrm{BR_{se}}$	0.51	0.053		
	Standing	$\mathrm{BR_{st}}$	0.57	0.053		
	Light activity	$\mathrm{BR_l}$	1.24	0.12		
	Moderate activity	$\mathrm{BR_m}$	1.77	0.37		
	Heavy activity	$\mathrm{BR_h}$	3.28	0.72		
	Viral load	vl	6.6	1.7	$\log_{10}$ RNA copies $\mathrm{mL^{-1}}$	Gaussian Kernel Density Estimation from dataset [25]

[a] Unit conversion might be necessary to compute qR

3 Occupation and activity profiles

The model supports a piecewise occupation profile where both the infected or exposed hosts can migrate in and out of the room at a given time, representing a close to real-life occupancy. In addition, we included a set of default activity profiles in terms of vocalisation activity and physical effort, which provide a weighted average of quantum emissions, depending on the type of activities performed in each scenario.

The scenarios chosen in this study, and their respective baseline activity, adopted measures and geometric parameters, are summarized in Table 5. The baseline preventive measures are not a representation of any particular real-life scenario, and shall not be used as a comparison with actual settings nor to the local public health related measures. We consider that during the breaks, the occupants leave the room and do not gather together in another indoor space, i.e. it considers a lapse of time where the occupants are not exposed to any airborne viruses.

To benchmark our model we used a case study of the epidemiological investigation on the Skagit valley chorale outbreak, by Miller at al. [19]. The outbreak recorded an attack rate between 53% and 87%, and the study indicated an estimated quantum generation rate of 970 $\mathrm{q\,h^{-1}}$.

4 Results and discussion

4.1 Quantum generation rate and infectious dose

The results of the probabilistic approach to the quantum generation rate qR, described in Section 2.5, are shown in Fig. 7 and Fig. 8. The average quantum generation rate for breathing (considering all

Table 5: Baseline Scenarios used in the study. The preventive measures are not a representation of any particular real-life scenario, and shall not be used as a comparison with actual settings nor to the local public health related measures. The default conditional probability of infection is calculated at $P(I|\text{qID} = 60)$, except for the Skagit valley chorale outbreak scenario which is calculated at $P(I|\text{qID} = 100)$ to compare with the same strain in circulation at that time.

Baseline Scenario	**Activity**	**Occupation**	**Ventilation**	**Face covering**	**Volume (m^3)**	$\mathbf{P(I|qID)}$	**N**
Shared office	Office-type: - Speaking $1/3$ of the time, seated Indoor RH < 40%	4 occupants; 1 infector: - 8h workday exposure - Lunch + 2 coffee breaks	Periodic opening of windows (10min every 2h), during winter	Surgical Mask	50	11%	0.33
Classroom	Training-type: - Teacher: speaking, light activity -Students: breathing, seated Indoor RH < 40%	20 occupants; 1 infector (teacher): - 8h class - Lunch break + 2 yard breaks	Periodic opening of windows (10min every 2h), during winter	-	160	36%	6.84
Ski cabin (see Fig. 6)	Confined-type: - Speaking, moderate activity Indoor RH > 40%	4 occupants; 1 infector: - 20 min ride	-	Surgical Mask	10	16%	0.48
Gym	Fitness-type: - Breathing, heavy activity Indoor RH > 40%	30 occupants; 2 infectors: - 60 min session	Mechanical 6 ACH	-	300	2%	0.56
Waiting room	Public administration-type: - Speaking 20% of the time, seated Indoor RH > 40%	15 occupants; 1 infectors: - 2h exposure	-	-	100	10%	1.4
Benchmark scenario: Skagit valley chorale outbreak [19]	Singing-type: - Shouting, light activity Indoor RH > 40%	61 occupants; 1 infector: - 2h30m exposure	Mechanical 0.7 ACH	-	810	32% [a] 79% [b]	21 45

[a] Values assuming $\text{qID} = 100$ and calculated according to Eq. (20)

[b] Values assuming $\text{qID} = 100$ and calculated at its 80^{th} percentile, to outline the effect of a 'superspreading event'.

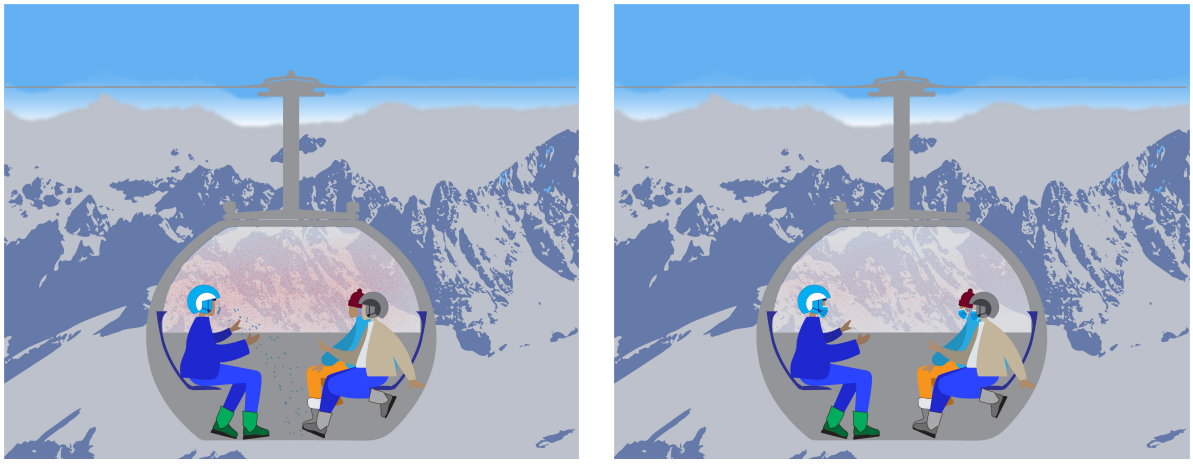

(a) Without masks

(b) With masks

Figure 6: Example illustration of a ski cabin on the way up the mountain while occupants are a) wearing masks and b) not wearing masks. The red dots represent the infectious airborne particles and in blue larger droplets. From a) to b) one can visualize the effect on capturing the large droplets and the reduction of airborne particles by roughly half.

physical activities) is substantially lower compared to speaking and shouting (factor of 75 and 377 less) which explains the importance of vocalisation in the airborne transmission of respiratory viruses. In this section, we adopt the notation "median [90% CI: 5^{th} percentile - 95^{th} percentile]" to give an immediate description of the histograms related to the samples generated by Monte Carlo simulation (MCS). This way, the median values and the limits of a 90% confidence interval (CI) of qR for shouting and a light physical activity are 43 [90% CI: 0.02- 7400], 8 [90% CI: 0.003 - 1500] and 4 [90% CI: 0.002 - 740] q h^{-1} for qID equal to 100, 500 and 1000 RNA copies q^{-1}, respectively. As expected, the distribution of qR is highly governed by the range of viral load data used in the simulation (Fig. 7). Although one could define boundaries to reduce the variability of the data, we would lose the real-life effects on the particular dynamics of this disease. Comparing these results with the Skagit Valley Chorale superspreading event [19], where the authors estimated a $\mathrm{qR} = 970 \pm 390q\ h^{-1}$, this would correlate in our data for someone shouting, light activity and in the range of the 80^{th} percentile for a qID = 100, i.e. $F^{-1}_{\mathrm{qR}|\mathrm{qID}=100}(0.8) = 1080q\ h^{-1}$, where $F^{-1}_{\mathrm{qR}|\mathrm{qID}=100}(\cdot)$ is the inverse conditional CDF of qR for qID = 100. Quantum generation rates were reported for other respiratory viruses and show good agreement with the results from the model showing that the mean quantum generation rate for breathing is below the estimated range for Influenza in an airplane outbreak [18] and for Measles in a school outbreak [14]. As mentioned above, the effect of vocalisation dramatically increases the generation of quanta per unit time, bringing the values comparable with recorded outbreaks for Measles and the upper limit of Tuberculosis [76] (cf. Fig. 9).

These results indicate that one SD from the mean increases qR by approximately 2 orders of magnitude: mean = 1.4 $\log_{10}$ (q h^{-1}) and mean + 1SD = 3.1 $\log_{10}$ (q h^{-1}), for qID of 100 RNA copies q^{-1}. This is also consistent with the existence of super-emitters causing superspreading events [77], where a small fraction of individuals are found to emit much more particles than others [21, 78, 79]. The combination of super-emitters with high viral loads are a recipe for superspreading events causing a high attack rate of new infections, such as the Skagit Valley Chorale. Therefore, we conclude our model benchmarks the results in [19] assuming a qID of 100 RNA copies for a non-VOC, so that the attack rate can be expressed as $P(I|\mathrm{qID} = 100)$.

Regarding the different virus variants and their qID, the result of tuning the infectious dose such that the effective reproduction number with VOC 202012/01 is 55% higher (cf. Section 2.1.4) yields the

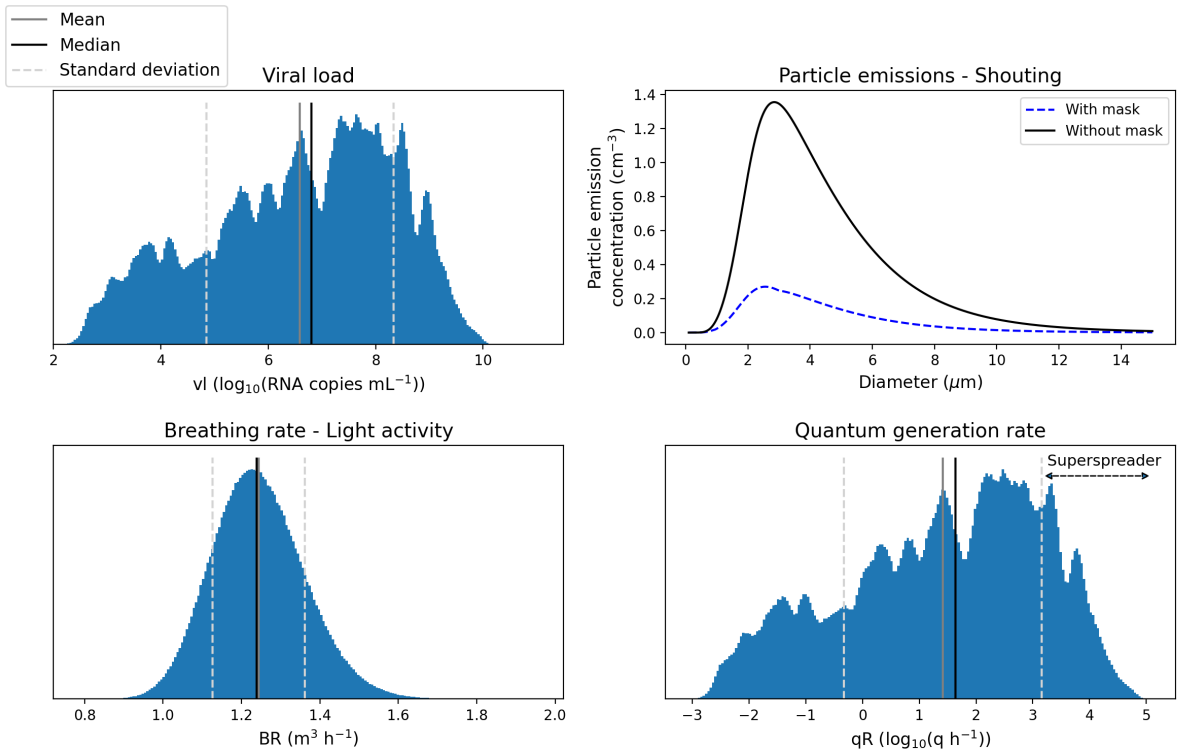

Figure 7: Results of the MCS for the determination of the quantum generation rate distribution for an infected host shouting, while undertaking light physical activity and assuming a qID = 100. The vertical axis of the three histograms correspond to the estimation of distribution PDFs. The median qR value is 43 q h^{-1} with a mean (SD) of 1.4 (1.7) $\log_{10}$(q h^{-1}). The superspreader range is represented by the values one standard deviation from the mean, where qR > 1400 q h^{-1}. Results computed from a 200 000 sample Monte Carlo simulation; the data used is described in Section 2.1 and associated subsections.

following ratio:

$$\frac{\mathrm{qID}_{B.1.1.7}}{\mathrm{qID}_{non-VOC}} = 0.6, \tag{21}$$

which returns an estimated infectious dose of 60 RNA copies q^{-1}, hence the conditional probability $P(I|\mathrm{qID} = 60)$ in Eq. (20) would correspond to $P(I)$ from Eq. (19), for hosts infected with VOC 202012/01. This was achieved simulating a large community outbreak, with 60 occupants (in which one was infected) where the ratio between the basic reproduction numbers using $\mathrm{qID} = 100$ and $\mathrm{qID} = 60$ resulted in a 55% increase in transmission. Due to the prevalence of the VOC at the time of writing, we assume a default infectious dose qID of 60 RNA copies q^{-1}, unless specified otherwise. This way and for the sake of simplification, in the following, we will indicate with $P(I)$ the conditional probability $P(I|\mathrm{qID} = 60)$ and, analogously, with $P(I|\mathrm{vl})$ the conditional probability $P(I|\mathrm{vl}, \mathrm{qID} = 60)$, unless specified otherwise.

It should be noted that the conditional approach for qID is considered to be a fragile aspect of the model that can be tuned once further data is published.

The effect of source control masks yields a reduction of the median qR by a factor of 5.4 - qR without masks: 43 [90% CI: 0.02 - 7400]; qR with masks: 7.9 [90% CI: 0.03 - 1349] $\log_{10}$(q h^{-1}). This is in agreement with Asadi et al. studied the effect of particle emissions with surgical masks and measured a factor 6 reduction [47].

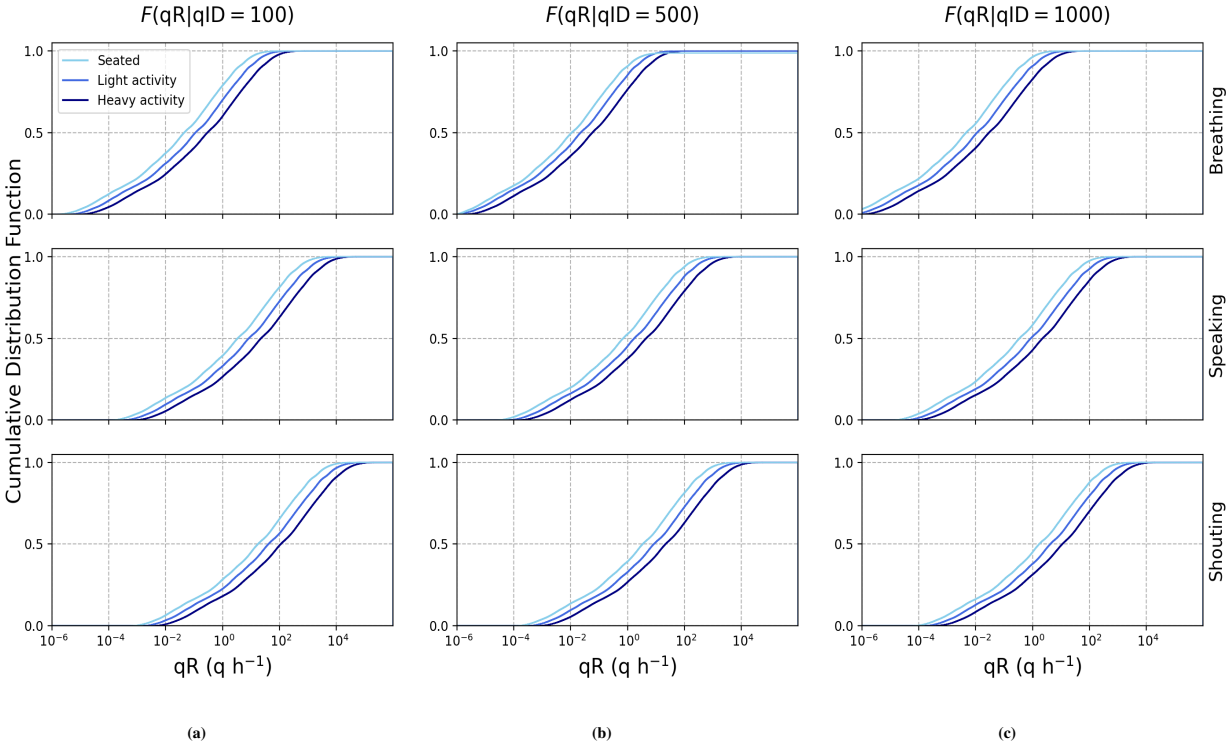

Figure 8: Estimation of the conditional cumulative probability of qR based on 200 000 MCSs for different expiratory activities (Breathing, Speaking and Shouting - from top to bottom) and different physical activities (Seated, Light and Heavy activity), given an estimated quantum infection dose qID of (a) 100, (b) 500 or (c) 1000 RNA copies per q. The values are without the effect of face covering ($\eta_{\text{out}} = 0$).

4.2 Concentration profiles and probability of infection

The successive application of Eqs. (2) and (5) to the samples of $\mathrm{BR_k}$ and vl, generated by MCSs on the distributions in Table 4, permits to obtain corresponding samples of the quantum concentration $C(t)$ and, therefore, to estimate its mean and significant percentiles at a given time. Following this approach for the the classroom scenario, we obtain the results presented in Fig. 10, which shows the quantum concentration over the exposure time, assuming a homogeneous mixture reaching a mean peak concentration of 2.37 [90% CI 0.07 - 12.4] q m^{-3}. Once again the wide confidence interval is governed by the viral load distribution, as previously discussed.

The results for the stochastic determination of the probability of infection from an exposure to VOC 202012/01, and consequent new cases N, for each baseline scenario can be found in Table 5). This provides a clear indication of the importance of proper ventilation and face coverings in the dissemination of the virus, in particular when in combination with events attended by many occupants. Once again the results are in agreement with our benchmark outbreak scenario, namely the Skagit Valley Chorale [19]. The outbreak had an estimated attack rate in between 53-87% [19], whereas our model predicts an infection probability of 32%. On the other hand, taking rather the 80^{th} percentile to outline the effect of a 'superspreading event', one get a probability of infection of 79%. Scenarios with neither efficient exchange with fresh air nor mask-wearing policies, yield the largest probabilities of infection.

Recent guidance has emerged to encourage natural ventilation in classrooms [81], although, in practice the use of natural ventilation via open windows might be found to be either i) uncomfortable for children due to low outdoor temperatures during the winter or ii) insufficient air ingress due to temperature equilibrium between indoor and outdoor air during the summer. The best solution would be to equip schools with properly sized mechanical HVAC systems, although it is sometimes complicated to perform retrofitting works within existing installations. A quick, easy, affordable and effective solution would be

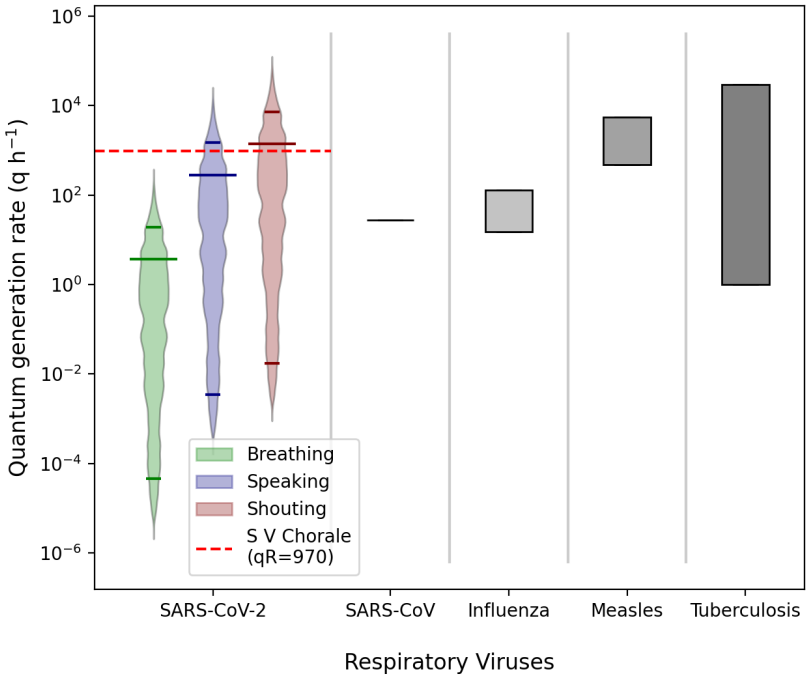

Figure 9: Comparison of the quantum generation rates reported in different outbreaks (Wells-Riley model) with the results of this study. **SARS-CoV-2** reflects the results from MCSs for a light physical activity and different expiratory activities (Breathing, Speaking, Shouting), assuming an infectious dose qID $= 100$ RNA copies q^{-1}. The violin plots denote the histograms of qR, with the bottom and top bars indicating the 5^{th} and 95^{th} percentiles and the larger bar in-between indicating the mean. The red dashed line indicates the outcome of the Skagit Valley Chorale outbreak study [19]. For the other respiratory viruses shown in the x-axis, the grey bars illustrate the range of qR reported for different outbreaks. **SARS-CoV**: outbreak in hospital - estimated qR: 28 q h^{-1} [80]; **Influenza**: outbreak in an airplane flight - estimated qR: 15 - 128 q h^{-1} [18]; **Measles**: outbreak in a school - estimated qR: 480 - 5580 q h^{-1} [14]; **Tuberculosis**: several outbreaks in clinical settings - estimated qR: 1 - 30000 q h^{-1} [76].

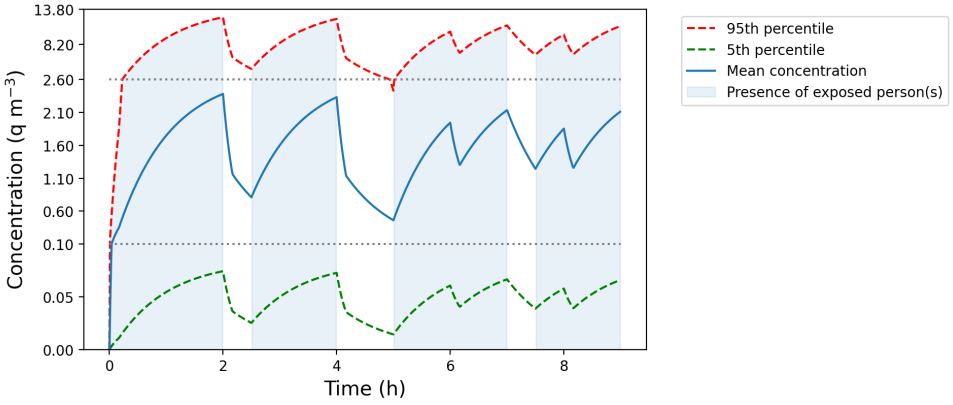

Figure 10: Results of the quantum concentration profile over the exposure time in the classroom scenario. The solid blue curve represents the mean concentrations with the dashed lines representing the 90% CI (5^{th} percentile - green curve; 95^{th} percentile - red curve). The blue shaded area illustrates the independent exposures block (i) mentioned in Eq. (16), during which the occupants are indeed exposed to the airborne viruses. Consequently, the white gaps correspond to the breaks where the occupants leave the room.

the use of HEPA filters. Installing HEPA filters ensuring, as a minimum, $\lambda_{HEPA}(0.8) = 5\ h^{-1}$, would reduce the mean absorbed quantum dose by a factor of 5.3 compared to no natural ventilation $-$ qD windows closed = 4.8 q [90% CI: 6×10^{-5} - 25]; qD with HEPA = 0.9 q [90% CI: 1×10^{-5} - 4.9], and a factor of 4.3 compared to the baseline scenario of periodically opening the windows every 2 hours for 10 minutes $-$ qD baseline = 3.9 q [90% CI: 5×10^{-5} - 21]; qD with HEPA = 0.9 q [90% CI: 1×10^{-5} - 5] (Fig. 11a). Measurements performed in school classrooms reported a similar result showing that inhaled

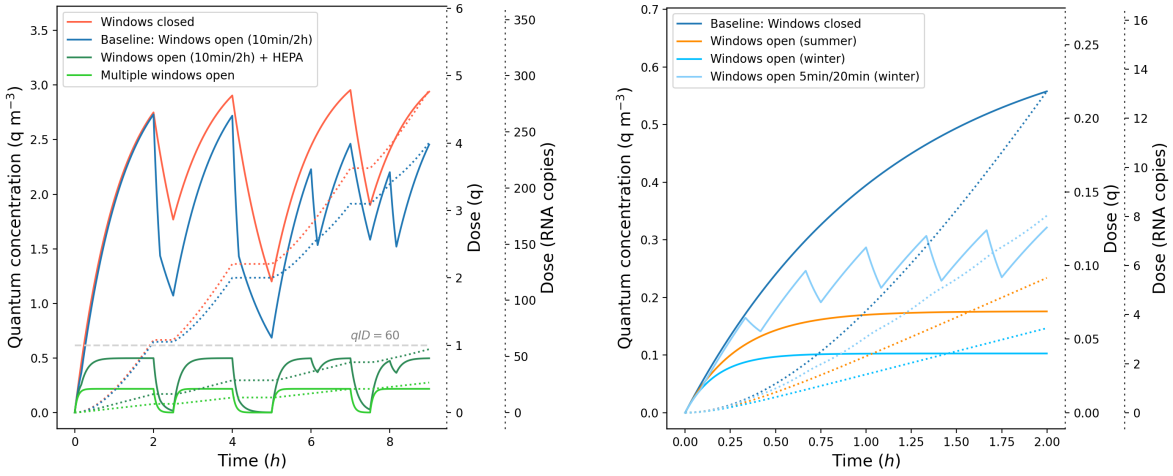

(a) Classroom scenario - Mean of $C(t)$ and qD

(b) Waiting room scenario - Mean of $C(t)$ and qD

Figure 11: Illustration of the estimated mean quantum concentration profile $C(t)$ over the exposure time and consequent estimated mean quantum dose qD absorbed by the exposed host, for different combination of measures represented by the different colors. The solid lines represent the concentration (left y-axis) and the dotted lines represent the cumulative quantum dose (right y-axes) which is shown both in unit quantum "q" or RNA copies. (a) Results for the classroom scenario. The horizontal dashed line denotes the quantum infectious dose limit. Time = 2 h corresponds to a 30 min yard break and first window opening for 15 min (if applicable); time = 4 h to a 1 hour lunch break and second window opening for 15 min (if applicable); time = 6 and 8 h to a third and fourth window opening for 15 min (if applicable); time = 7 h to a second 30 min yard break. (b) Results for the waiting room scenario. The drops in the curve with the periodic venting correspond to opening the window every 20 min for a duration of 5 min.

dose is reduced by a factor of 6 when using air purifiers at 5.7 h^{-1} [82]. Moreover, simply with either installing a HEPA filter or maintaining multiple (four) windows open permanently, one would get a mean qD lower than 1 q, i.e. one would not reach the infectious dose of 60 RNA copies q^{-1} (VOC 202012/01). The results also show that opening the windows for 10 minutes every 2 hours is not an efficient natural ventilation strategy since the mean qD would reach the infectious dose before the first yard break (i.e. after 2h in the classroom). Deciding to open multiple windows permanently, reduces the mean qD by a factor of 9.8 compared to the baseline $-$ qD baseline = 3.9 q [90% CI: 5×10^{-5} - 21]; qD with multiple windows = 0.4 q [90% CI: 6×10^{-6} - 2.3].

The other scenario which deserves attention is the waiting room, which could well be equivalent to any public setting where the volume is small, multiple people are present and without proper ventilation nor face coverings. Due to the relatively low exposure time (2h), the individual full infection probability $P(I)$ might seem quite low, yet the event scenario would not be effective in breaking the chain of transmission since $N = 1.45 > 1$. As discussed above, a valid solution is the installation of HEPA filters or a sound natural ventilation strategy. Despite a universal promotion of natural ventilation, the practical implementation and associated guidance are often conflicting. Several nations in Europe provided different guidance with respect to the opening of windows for natural ventilation [83], ranging from the periodic opening of windows for 10 to 15 minutes twice a day or simply opening the windows every 20 min. The duration and frequency of venting, as well as the temperature difference and wind incidence, is crucial for a sufficient air exchange and thus reducing the concentration of viruses (cf. Section 2.2.2.1). Our study suggests that a few openings during the course of the day (e.g. > 4-5 times per 8h) is comparable to not opening the windows at all for cases in which the equilibrium concentration without ventilation is very high (Fig. 11). To achieve results comparable with permanently opened windows, the periodicity of frequent venting should be high, i.e. every 15 to 20 minutes (Fig. 11b).

In addition to the periodicity of opening the windows, the temperature difference between outdoor and indoor air also plays a role. For the waiting room scenario, opening the windows during the winter

would yield a mean qD of approximately 0.06 q [90% CI: 7×10^{-7} - 0.3] which is about a factor 3.7 reduction compared to having the windows closed, i.e. a mean qD of approximately 0.22 q [90% CI: 3×10^{-6} - 1.1]. For an equivalent venting during the summer period the reduction factor falls to 2.4 with a mean qD of approximately 0.09 q [90% CI: 1×10^{-6} - 0.5]. This concludes that natural ventilation is approximately twice as effective during the winter than during the summer. These findings are consistent with the analytical approach, where the removal rate λ_{ACH} is proportional to $\sqrt{\Delta T}$ (see Eq. (8) – ΔT being 10 K in winter vs. 2 K in summer), slightly compensated by the lower biological removal rate λ_{bio} in the winter due to the effect of low RH. If one would need to prioritize the requirements and streamline the ventilation guidelines, the prescriptions should be towards leaving the windows open at all times independently of the season, since a window open during the summer is more efficient than a periodic venting for 5min every 20 min during the winter (Fig. 11b) - once the windows are closed the concentration increases at a faster rate achieving a higher value the next time the window opens. To summarize, natural ventilation is less effective during the summer period, although still more effective than the most conservative periodic venting scenario in Ref. [83] (i.e. frequent opening every 20min), as shown in Fig. 11. Natural ventilation is, nonetheless, very important and our study would suggest leaving the windows open at all times for maximum viral removal efficiency.

Analysing the effect of natural ventilation from a slightly different angle, a study has shown that higher airborne pollen concentrations might have an effect on increased infection rates [84]. Hence, opening the windows during the local pollen season may also induce a second order, detrimental effect on the infection probability which is not included in this study. However, it is safe to say that HEPA filtration will also help in reducing the pollen load in a given volume providing an extra mitigation measure to this effect. A further study could aim at including the pollen load as a variable in the model.

This study also enabled analysis of some interesting relationships with viral load during transmission. The conditional probability of transmitting the disease to other occupants $P(I|\text{vl})$ for a given viral load value in a defined indoor environment can be discussed by analysing 3 different zones in Fig. 12. For viral loads below a critical value $\text{vl}_{0.05}$, the probability of infection is close to 0%, whereas above $\text{vl}_{0.95}$ the probability is close to 100%. This demonstrates the aforementioned importance of the viral load of the infected host at the time of transmission, for the chances in breaking the chain of transmission - i.e. reaching $P(I) \approx 0$. The threshold values $\text{vl}_{0.05}$ and $\text{vl}_{0.95}$ depend on the effectiveness of the prevention measures. By adding stricter measures the $P(I|\text{vl})$ graph would move to the right, whereas relaxing the measures would shift the values to the left. Therefore, a less conservative approach in terms of preventive measures would increase the likelihood of infectious hosts with lower viral loads in transmitting the disease, as shown in Fig. 13.

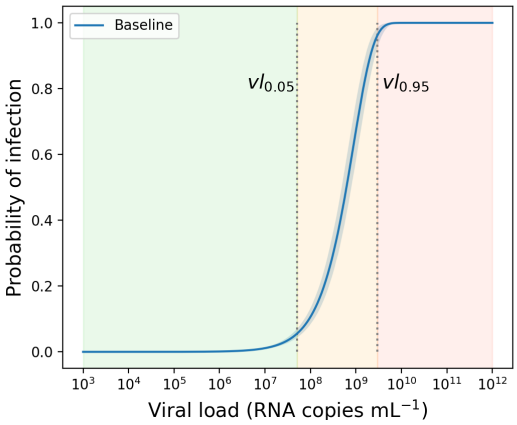

Figure 12: Conditional probability of infection $P(I|\text{vl})$ (shared office scenario), with a 98% CI (blue shaded area). $\text{vl}_{0.05} = 10^{7.8}$ and $\text{vl}_{0.95} = 10^{9.5}$ are the critical viral load values for which $P(I)$ = 5% and $P(I)$ = 95%, respectively, dividing the range of viral loads into three shaded regions (in green, orange and red).

The data also indicates that the probability of infection follows a quasi-binary relationship, i.e., for a given scenario either transmission will not occur ($P(I) \approx 0$) or will occur ($P(I) \approx 1$). This can be observed by analysing the histograms in Fig. 13a - 13b (iii), where the majority of the samples generated by MCSs on viral load distribution leads to a value of $P(I|\text{vl})$ in the neighborhood of the lower and upper bounds 0 and 1. The probability of falling within the orange zone in the baseline

scenario ($\mathrm{vl}_{0.05} < \mathrm{vl} < \mathrm{vl}_{0.95}$) is 28%, which is spread throughout the range $0.05 < P(I|\mathrm{vl}) < 0.95$. It is understood that the detection of viral RNA copies does not necessarily mean an equal amount of viable virus (i.e. virions), although the results of this study strikingly correlate to the findings of van Kampen et al. [85] where the probability of isolating infectious SARS-CoV-2 viruses in RNA samples starts to increase with viral loads larger than 10^6 RNA copies mL^{-1}, reaching a probability of approximately 90% at 10^{10} RNA copies mL^{-1}. In our study, the rise in probability of infection for several baseline scenarios also occurs at viral loads higher than 10^6 RNA copies mL^{-1}.

A deeper analysis of Fig. 13 reveals the importance of introducing appropriate measures that would shift the curves in plot (i) towards the right. Hypothetically, by splitting the $P(I|\mathrm{vl})$ curve in half (i.e. at $P(I|\mathrm{vl}) = 0.5$) and analysing the distribution of viral load samples to left and to the right of the dotted line (i.e $\mathrm{vl} < \mathrm{vl}_{0.5}$ & $\mathrm{vl} > \mathrm{vl}_{0.5}$ in Fig. 13a - 13b (ii)), we can promptly see the result in the histogram of the values of probability of infection in Fig. 13a - 13b (iii). Relaxing preventive measures (i.e. shifting the curve to the left) would yield higher density of samples close to $P(I) \approx 1$ and therefore increase the chances of transmitting the disease. This also shows the importance and effectiveness of large scale diagnostics in asymptomatic or presymptomatic hosts early into their infection, so that they are placed in isolation before the viral load increases beyond the critical level. This confirms early studies analysing epidemiological data where fast tracking and isolation reduces the spread [86].

Approximately 80% of the samples in Ref. [25] were found to detect viral loads less than 10^8 RNA copies mL^{-1} and approximately 95% less than 10^9 RNA copies mL^{-1}, therefore by tuning the correct measures tailored for each indoor setting such that $\mathrm{vl}_{0.95} \geq 10^9$, the risk assessment of airborne transmission could be considered as acceptable. The residual risk linked to the remaining 5% of viral loads above 10^9 RNA copies mL^{-1} might not be acceptable to settings with a combination of situations which are propitious for superspreading events, such as Crowded, Close-contact and Confined settings - three C's (3C), or for settings involving a large gatherings of people, such as conferences, social events or demonstrations. For such settings we recommend to either i) increase the threshold to $\mathrm{vl}_{0.95} \geq 10^{10}$ RNA copies mL^{-1}, which would probably require a non-negligible upgrade of venue layouts and ventilation systems, or 2) in addition to ensuring $\mathrm{vl}_{0.95} \geq 10^9$, include a rapid antigen testing strategy of the participants. The latter option would cover the residual risk of infected hosts with high viral loads (>10^9) participating in the event. Antigen detection assay for SARS-CoV-2 is found to be most effective in hosts with high viral loads, regardless of symptoms, reaching a sensitivity of 93.3% and specificity of 99.9%, for an equivalent RT-PCR Ct < 30, corresponding a viral load as low as 1.6x10^4 RNA copies mL^{-1} [87].

For shared offices, a baseline scenario including the use of masks and periodic venting, is considered acceptable since it is not deemed as a 3C setting and on the provision that these two measures are combined simultaneously. Although, relaxing these two measures would increase the risk beyond the notion of acceptable, i.e. $\mathrm{vl}_{0.95} = 10^{8.5}$ RNA copies mL^{-1} (Fig. 13a).

For the classroom scenario (Fig. 13b), the situation where a HEPA filter is installed, while maintaining a periodic natural ventilation strategy, just falls short of the threshold $\mathrm{vl}_{0.95} = 10^{8.8}$ RNA copies mL^{-1} yielding a probability $P(I)$ of approximately 22.7%. Opening multiple windows alone or with the inclusion of surgical masks would improve the situation and reach $\mathrm{vl}_{0.95} \geq 10^9$ with an estimated $P(I)$ of approximately 16.3% and 4.4%, respectively. The importance of natural ventilation is demonstrated where the probability of infection can be reduced by about 22 percentage points just by opening permanently the windows and an additional 12 by prescribing the use of surgical-type masks. Figure 13b confirms that a periodic opening strategy of windows is not ideal.

Some countries opted to keep ski resorts open during the widespread COVID-19 restrictions. In this study we look at the potential risk of airborne transmission in cabins for ski lifts (Fig. 6). For a typical 10 m^3 cabin, the recommended maximum travel time is approximately 20 minutes with surgical type masks (Fig. 14). The duration of the time to which the occupants are exposed to the viral concentration could play an important factor in decreasing transmission. In the ski cabin scenario, the travel time should be reduced to approximately 7 minutes if the occupants are not wearing masks (Fig. 14b),

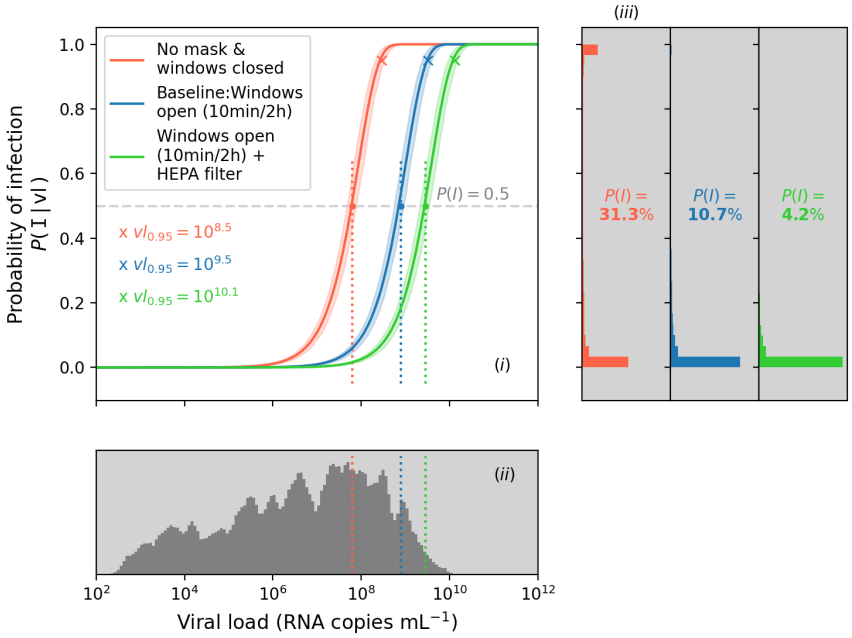

(a) Shared office scenario

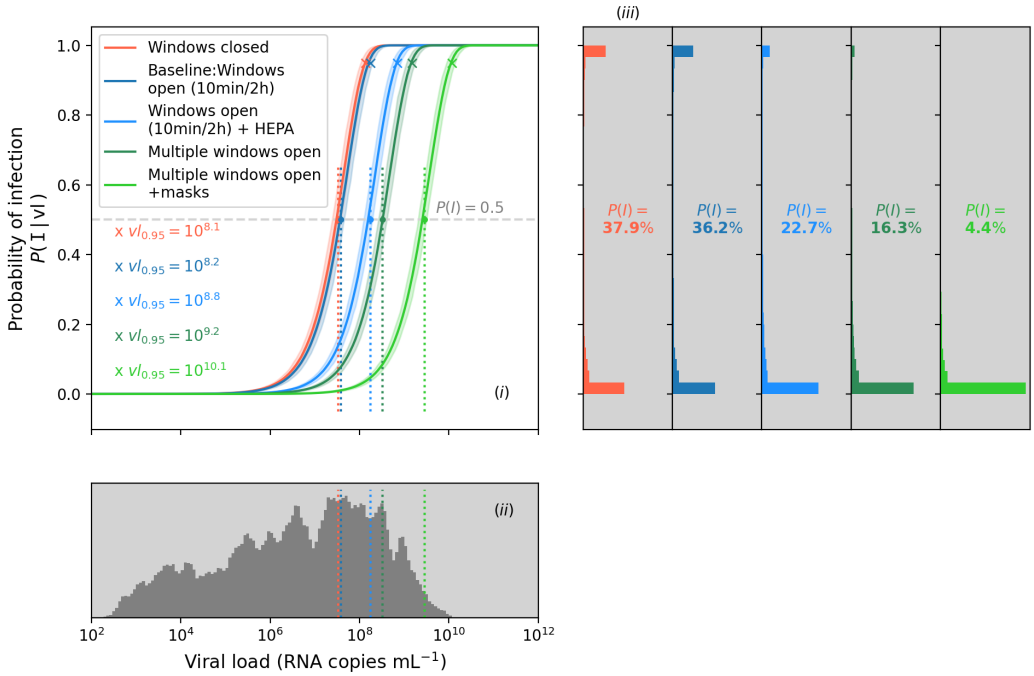

(b) Classroom scenario

Figure 13: Probability of infection in the shared office and classroom scenarios, and related dependency on the viral load. **(a)** For the shared office scenario and **(b)** for the classroom scenario. In each of the 2 figures: **(i)** Expected probability of infection for a given viral load value, with a 98% CI (shaded area). Comparison between the baseline scenario (dark blue curve) and situations with stricter or relaxed set of measures. The baseline scenarios are given in Table 5. The 'x' markers denote the critical viral load $\mathrm{vl}_{0.95}$ in each situation. The dotted lines correspond to the intersection of each curve with $P(I|\mathrm{vl}) = 50\%$. **(ii)** Histogram of the viral load data from [25]. The vertical axis corresponds to the probability density function of the adopted distribution. The dotted lines indicate the contribution of the viral load samples for reaching $P(I|\mathrm{vl})$ greater than 50% (i.e. samples to the right of the dotted line) and lower than 50% (i.e. samples to the left of the dotted line), for each situation. **(iii)** Set of histograms of the conditional probability of infection $P(I|\mathrm{vl})$, one for each situation, showing the results of the MCSs, including the integration on the full range of viral load data in [25], which gives the $P(I)$ value (as per Section. 2.5) shown in the middle of each histogram plot.

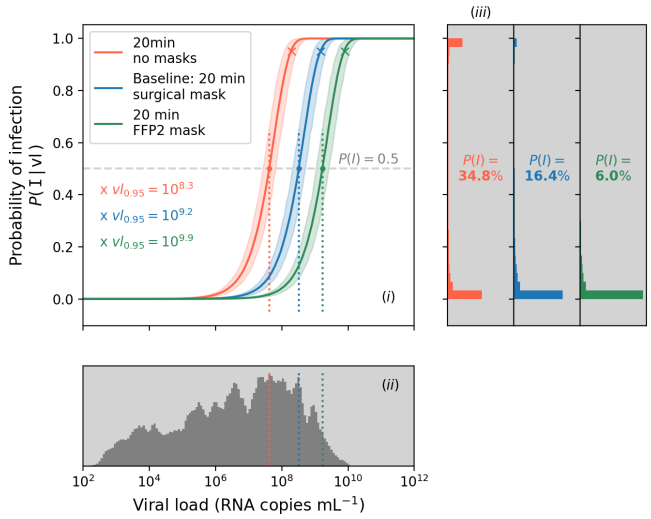

(a) Ski cabin scenario: infection probability vs viral load

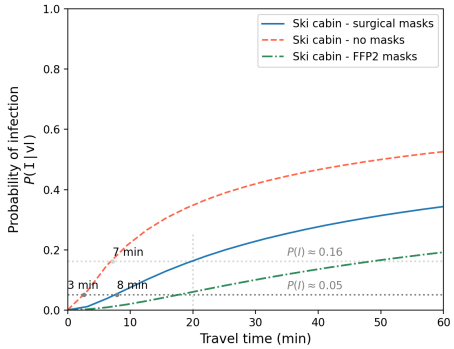

(b) Ski cabin scenario: infection probability vs exposure time

Figure 14: Comparison of the ski cabin scenario by ranging the exposure time inside. **a)** Probability of infection and related dependency on vl. **(i)** Expected probability of infection for a given viral load value, with a 98% CI (shaded area). Comparison of baseline scenario (blue curve) and different travel times. The baseline scenario is given in Table 5 where ski lift takes 20 min and the occupants are wearing masks. The 'x' markers denote the critical viral load $\mathrm{vl}_{0.95}$ in each situation. The dotted lines correspond to the intersection of each curve with $P(I|\mathrm{vl}) = 50\%$. **(ii)** Histogram of the viral load data from [25].The vertical axis corresponds to the probability density function of the adopted distribution. The dotted lines indicate the contribution of the viral load samples for reaching $P(I|\mathrm{vl})$ greater than 50% (i.e. samples to the right of the dotted line) and lower than 50% (i.e. samples to the left of the dotted line), for each situation. **(iii)** Three histograms of the values of the conditional probability of infection $P(I|\mathrm{vl})$, one for each situation, showing the results of the MCSs, including the integration on the full range of viral load data in [25], which gives the $P(I)$ value (as per Section 2.5) shown in the middle of each histogram plot. **b)** Effect of the exposure time on the infection probability $P(I)$ if the occupants do not wear masks, compared to wearing surgical or FFP2 type masks. The horizontal dotted lines correspond the the potential level of acceptable risk: $P(I)$=16% represents the level at which the viral load threshold $\mathrm{vl}_{0.95}$ is reached (Fig. 14a) and $P(I)$=5% represents a more conservative risk level.

although this situation would imply a potential risk of short-range airborne exposure due to the small interpersonal distance in the cabin. Hence, the results without masks should be taken with caution as it may underestimate the transmission probability in this particular setting. If the resort or local authorities deem necessary to reduce even further the acceptable risk level, e.g. to 5%, the maximum travel time would reduce to 8 min instead of 20 min. To accept a 20 min exposure, while maintaining a conservative risk level, the occupants would have to (properly) wear respirators such as FFP2 masks. For a hypothetical 1 hour exposure, e.g. during a technical fault of the ski lift, the probability of infection would raise to approximately 34% in the case of using surgical masks and 53% in the case of no masks.

Ski cabins generally have a small opening on one side, although if we assume that the volume is not actively heated (e.g. sensible heat from radiators) or passively heated (e.g. latent heat from the occupants), the outdoor and indoor air temperature can be assumed to be in equilibrium. Hence the effect of removal rate from natural ventilation (including infiltration) is neglected, as a conservative approach.

5 Conclusions

Just like any other occupational health and safety risk, it is of vital importance to fully understand the hazards and explain the rationale behind the preventive measures. A proper understanding of how respiratory viruses are transmitted is an essential step towards ensuring proper protection. This paper focuses on describing the airborne transmission mode of SARS-CoV-2 and proposing an engineering approach to assess the most suitable preventive and protective measures.

Facility managers, health and safety professionals, as well as individuals must systematically address the new paradigm of including the risk of airborne transmission of respiratory viruses as a seri-

ous occupational hazard. If possible, they should have easy access to simplified models, like the one presented in this paper, to perform the required analysis to estimate the risk level in their particular indoor setting(s). Although the notion of acceptable risk depends on national legislation and corporate/organisational risk management strategies, this paper provides some guidance on how to determine whether or not the risk of airborne transmission is mitigated. We propose a simplified model, called the COVID Airborne Risk Assessment (CARA), that allows for a quick and efficient assessment of the control volume and used epidemiological outbreaks, measurement and other published findings to benchmark our results. The fact that the model is 'quick and efficient' relates to some of the assumptions and consequent limitations that were discussed above with the inclusion of proper physical justifications.

While performing such risk assessments, the aim should be focused on ensuring that the indoor setting is not contributing to the spread of the virus and thus having the number of new cases arising from an infected host $(N) < 1$. In addition, the individual probability of infection $P(I)$ should also be low enough so that the critical viral load is below 10^9 RNA copies mL^{-1} for nominal scenarios. For settings with a combination of crowded, close-contact and poorly ventilated areas, additional measures, such as the inclusion of rapid antigen testing strategies or increasing the threshold to 10^{10} RNA copies mL^{-1}, are recommended wherever possible. For these cases, facility managers can tune the preventive measures so that this risk is controlled.

The present study is highly dependent on the viral load data and associated statistical descriptors. The use of other datasets would have an impact on the results, which might consequently impact the findings of this study. Nonetheless, the authors were cautious to choose a distribution that would represent a broad envelope by taking data during the expansionary phase of the epidemic, yielding higher values compared to other less critical phases and thus representing a conservative assumption. The conditional approach towards the quantum infectious dose is employed due to the lack of specific scientific evidence. The authors substantiated their choices, although this could be considered as a vulnerable aspect of the model that can be tuned once further data is published.

This study shows that with a risk-based approach, the chances of contracting COVID-19 can be mitigated in existing infrastructure without major modifications or costly consolidations plans, by e.g. optimizing of the exposure time / occupation profile, ensuring sufficient natural ventilation adapted to the different temperature profiles or using adequate face covering measures. In a post-COVID era, we will face a new paradigm with the inclusion of this novel occupational hazard, using models and tools such as CARA to protect building occupants against airborne transmission of respiratory pathogens.

Acknowledgements

We wish to thank CERN's HSE Unit, Beams Department, Experimental Physics Department, Information Technology Department, Industry, Procurement and Knowledge Transfer Department and International Relations Sector for their support to the study. Thanks to Doris Forkel-Wirth, Benoit Delille, Walid Fadel, Olga Beltramello, Letizia Di Giulio, Evelyne Dho, Wayne Salter, Benoit Salvant and colleagues from the COVID working group for providing expert advice and extensively testing the model. Finally, we wish to thank Fabienne Landua and the design service for preparing the illustrations and Alessandro Raimondo, Ana Padua and Manuela Cirilli from the Knowledge Transfer Group for their continuous support.

Bibliography

[1] L. Morawska and D. K. Milton, "It Is Time to Address Airborne Transmission of Coronavirus Disease 2019 (COVID-19)," *Clinical Infectious Diseases*, vol. 71, pp. 2311–2313, 07 2020. https://doi.org/10.1093/cid/ciaa939.

[2] J. R. Port, C. K. Yinda, I. O. Owusu, *et al.*, "SARS-CoV-2 disease severity and transmission efficiency is increased for airborne but not fomite exposure in syrian hamsters," *bioRxiv*, 2020. https://doi.org/10.1101/2020.12.28.424565.

[3] C. J. Roy and D. K. Milton, "Airborne transmission of communicable infection — the elusive pathway," *New England Journal of Medicine*, vol. 350, no. 17, pp. 1710–1712, 2004. https://doi.org/10.1056/NEJMp048051.

[4] X. He, E. H. Lau, P. Wu, *et al.*, "Temporal dynamics in viral shedding and transmissibility of COVID-19," *Nature medicine*, vol. 26, no. 5, pp. 672–675, 2020. https://doi.org/10.1038/s41591-020-0869-5.

[5] M. Cevik, M. Tate, O. Lloyd, *et al.*, "SARS-CoV-2, SARS-CoV, and MERS-CoV viral load dynamics, duration of viral shedding, and infectiousness: a systematic review and meta-analysis," *The Lancet Microbe*, vol. 2, no. 1, pp. e13 – e22, 2021. https://doi.org/10.1016/S2666-5247(20)30172-5.

[6] M. Nicas, W. W. Nazaroff, and A. Hubbard, "Toward understanding the risk of secondary airborne infection: Emission of respirable pathogens," *Journal of Occupational and Environmental Hygiene*, vol. 2, no. 3, pp. 143–154, 2005. https://doi.org/10.1080/15459620590918466.

[7] C. J. Noakes and P. A. Sleigh, "Mathematical models for assessing the role of airflow on the risk of airborne infection in hospital wards," *Journal of The Royal Society Interface*, vol. 6, no. suppl_6, pp. S791–S800, 2009. https://doi.org/10.1098/rsif.2009.0305.focus.

[8] European Centre for Disease Prevention and Control, "Risk related to spread of new SARS-CoV-2 variants of concern in the EU/EEA," risk assessment, ECDC, Stockholm, Jan 2021. https://www.ecdc.europa.eu/en/publications-data/covid-19-risk-assessment-spread-new-sars-cov-2-variants-eueea.

[9] A. Rambaut, E. C. Holmes, Á. O'Toole, *et al.*, "A dynamic nomenclature proposal for SARS-CoV-2 lineages to assist genomic epidemiology," *Nature Microbiology*, vol. 5, no. 11, pp. 1403–1407, 2020. https://doi.org/10.1038/s41564-020-0770-5.

[10] L. Morawska, G. Johnson, Z. Ristovski, *et al.*, "Size distribution and sites of origin of droplets expelled from the human respiratory tract during expiratory activities," *Journal of Aerosol Science*, vol. 40, no. 3, pp. 256 – 269, 2009. https://doi.org/10.1016/j.jaerosci.2008.11.002.

[11] W. G. Lindsley, J. D. Noti, F. M. Blachere, *et al.*, "Viable influenza a virus in airborne particles from human coughs," *Journal of Occupational and Environmental Hygiene*, vol. 12, no. 2, pp. 107–113, 2015. https://doi.org/10.1080/15459624.2014.973113.

[12] W. Yang and L. C. Marr, "Dynamics of airborne influenza a viruses indoors and dependence on humidity," *PLOS ONE*, vol. 6, pp. 1–10, 06 2011. https://doi.org/10.1371/journal.pone.0021481.

[13] M. Moriyama, W. J. Hugentobler, and A. Iwasaki, "Seasonality of respiratory viral infections," *Annual Review of Virology*, vol. 7, no. 1, pp. 83–101, 2020. https://doi.org/10.1146/annurev-virology-012420-022445.

[14] E. C. Riley, G. Murphy, and R. L. Riley, "Airborne Spread of measles in a suburban elementary school," *American Journal of Epidemiology*, vol. 107, pp. 421–432, 05 1978. https://doi.org/10.1093/oxfordjournals.aje.a112560.

[15] G. Buonanno, L. Morawska, and L. Stabile, "Quantitative assessment of the risk of airborne transmission of SARS-CoV-2 infection: Prospective and retrospective applications," *Environment International*, vol. 145, p. 106112, 2020.
https://doi.org/10.1016/j.envint.2020.106112.

[16] W. F. Wells, *Airborne Contagion and Air Hygiene. An Ecological Study of Droplet Infections.* Cambridge : Harvard University Press (for The Commonwealth Fund), Mass., USA, 1955.

[17] G. N. Sze To and C. Y. H. Chao, "Review and comparison between the Wells–Riley and dose-response approaches to risk assessment of infectious respiratory diseases," *Indoor Air*, vol. 20, no. 1, pp. 2–16, 2010.
https://doi.org/10.1111/j.1600-0668.2009.00621.x.

[18] S. N. Rudnick and D. K. Milton, "Risk of indoor airborne infection transmission estimated from carbon dioxide concentration," *Indoor Air*, vol. 13, no. 3, pp. 237–245, 2003.
https://doi.org/10.1034/j.1600-0668.2003.00189.x.

[19] S. L. Miller, W. W. Nazaroff, J. L. Jimenez, *et al.*, "Transmission of SARS-CoV-2 by inhalation of respiratory aerosol in the skagit valley chorale superspreading event," *Indoor Air*, vol. 31, no. 2, p. 314– 323, 2021.
https://doi.org/10.1111/ina.12751.

[20] G. Johnson, L. Morawska, Z. Ristovski, *et al.*, "Modality of human expired aerosol size distributions," *Journal of Aerosol Science*, vol. 42, no. 12, pp. 839 – 851, 2011.
https://doi.org/10.1016/j.jaerosci.2011.07.009.

[21] S. Asadi, A. S. Wexler, C. D. Cappa, *et al.*, "Aerosol emission and superemission during human speech increase with voice loudness," *Scientific reports*, vol. 9, no. 1, pp. 1–10, 2019.
https://doi.org/10.1038/s41598-019-38808-z.

[22] V. Stadnytskyi, C. E. Bax, A. Bax, and P. Anfinrud, "The airborne lifetime of small speech droplets and their potential importance in SARS-CoV-2 transmission," *Proceedings of the National Academy of Sciences*, vol. 117, no. 22, pp. 11875–11877, 2020.
https://doi.org/10.1073/pnas.2006874117.

[23] J. Fajnzylber, J. Regan, K. Coxen, *et al.*, "SARS-CoV-2 viral load is associated with increased disease severity and mortality," *Nature Communications*, vol. 11, p. 5493, Oct 2020.
https://doi.org/10.1038/s41467-020-19057-5.

[24] Y. Pan, D. Zhang, P. Yang, *et al.*, "Viral load of SARS-CoV-2 in clinical samples," *The Lancet Infectious Diseases*, vol. 20, no. 4, pp. 411 – 412, 2020.
https://doi.org/10.1016/S1473-3099(20)30113-4.

[25] D. Jacot, G. Greub, K. Jaton, and O. Opota, "Viral load of SARS-CoV-2 across patients and compared to other respiratory viruses," *Microbes and Infection*, vol. 22, no. 10, pp. 617 – 621, 2020.
https://doi.org/10.1016/j.micinf.2020.08.004.

[26] K. K.-W. To, O. T.-Y. Tsang, W.-S. Leung, A. R. Tam, T.-C. Wu, D. C. Lung, *et al.*, "Temporal profiles of viral load in posterior oropharyngeal saliva samples and serum antibody responses during infection by SARS-CoV-2: an observational cohort study," *The Lancet Infectious Diseases*, vol. 20, no. 5, pp. 565 – 574, 2020.
https://doi.org/10.1016/S1473-3099(20)30196-1.

[27] C. Rothe, M. Schunk, P. Sothmann, *et al.*, "Transmission of 2019-nCoV infection from an asymptomatic contact in germany," *New England Journal of Medicine*, vol. 382, no. 10, pp. 970–971, 2020.
https://doi.org/10.1056/NEJMc2001468.

[28] N. G. Davies, S. Abbott, R. C. Barnard, *et al.*, "Estimated transmissibility and impact of sars-cov-2 lineage b.1.1.7 in england," *Science*, 2021.
https://doi.org/10.1126/science.abg3055.

[29] A. S. Walker, K.-D. Vihta, O. Gethings, *et al.*, "Increased infections, but not viral burden, with a new SARS-CoV-2 variant," *medRxiv*, 2021. https://doi.org/10.1101/2021.01.13.21249721.

[30] J. A. Hay, L. Kennedy-Shaffer, S. Kanjilal, *et al.*, "Estimating epidemiologic dynamics from cross-sectional viral load distributions," *medRxiv*, 2021. https://doi.org/10.1101/2020.10.08.20204222.

[31] M. Kidd, A. Richter, A. Best, *et al.*, "S-variant SARS-CoV-2 lineage B1.1.7 is associated with significantly higher viral loads in samples tested by ThermoFisher TaqPath RT-qPCR," *The Journal of Infectious Diseases*, 2021. jiab082, https://doi.org/10.1093/infdis/jiab082.

[32] K. K.-W. To, O. T.-Y. Tsang, W.-S. Leung, *et al.*, "Temporal profiles of viral load in posterior oropharyngeal saliva samples and serum antibody responses during infection by SARS-CoV-2: an observational cohort study," *The Lancet Infectious Diseases*, vol. 20, no. 5, pp. 565–574, 2020. https://doi.org/10.1016/S1473-3099(20)30196-1.

[33] Public Health England, "Investigation of novel SARS-COV-2 variant: Variant of concern 202012/01, technical briefing 1," tech. brief, PHE, London, 2020. https://www.gov.uk/government/publications/investigation-of-novel-sars-cov-2-variant-variant-of-concern-20201201.

[34] D. K. Milton, "A Rosetta Stone for Understanding Infectious Drops and Aerosols," *Journal of the Pediatric Infectious Diseases Society*, vol. 9, pp. 413–415, 07 2020. https://doi.org/10.1093/jpids/piaa079.

[35] M. Gameiro da Silva, "An analysis of the transmission modes of COVID-19 in light of the concepts of indoor air quality," *REHVA journal*, vol. 3, pp. 46 – 54, June 2020. https://www.rehva.eu/rehva-journal/detail/03-2020.

[36] R. S. Papineni and F. S. Rosenthal, "The size distribution of droplets in the exhaled breath of healthy human subjects," *Journal of Aerosol Medicine*, vol. 10, no. 2, pp. 105–116, 1997. https://doi.org/10.1089/jam.1997.10.105.

[37] L. Morawska, "Droplet fate in indoor environments, or can we prevent the spread of infection?," *Indoor Air*, vol. 16, no. 5, pp. 335–347, 2006. https://doi.org/10.1111/j.1600-0668.2006.00432.x.

[38] L. C. Marr, J. W. Tang, J. Van Mullekom, and S. S. Lakdawala, "Mechanistic insights into the effect of humidity on airborne influenza virus survival, transmission and incidence," *Journal of The Royal Society Interface*, vol. 16, no. 150, p. 20180298, 2019. https://doi.org/10.1098/rsif.2018.0298.

[39] E. Kudo, E. Song, L. J. Yockey, *et al.*, "Low ambient humidity impairs barrier function and innate resistance against influenza infection," *Proceedings of the National Academy of Sciences*, vol. 116, no. 22, pp. 10905–10910, 2019. https://doi.org/10.1073/pnas.1902840116.

[40] T. Watanabe, T. A. Bartrand, M. H. Weir, *et al.*, "Development of a dose-response model for SARS coronavirus," *Risk Analysis*, vol. 30, no. 7, pp. 1129–1138, 2010. https://doi.org/10.1111/j.1539-6924.2010.01427.x.

[41] R. H. Alford, J. A. Kasel, P. J. Gerone, and V. Knight, "Human influenza resulting from aerosol inhalation," *Proceedings of the Society for Experimental Biology and Medicine*, vol. 122, no. 3, pp. 800–804, 1966. https://doi.org/10.3181/00379727-122-31255.

[42] Department of Homeland Security (DHS) Science and Technology Directorate (S&T), "Master question list for COVID-19 (caused by SARS-CoV-2), required information for effective infectious disease outbreak response. last accessed 12 march 2021.," report, DHS (S&T), Washington DC, 2021.
https://www.dhs.gov/publication/st-master-question-list-covid-19.

[43] N. H. L. Leung, D. K. W. Chu, E. Y. C. Shiu, *et al.*, "Respiratory virus shedding in exhaled breath and efficacy of face masks," *Nature Medicine*, vol. 26, pp. 676–680, May 2020.
https://doi.org/10.1038/s41591-020-0843-2.

[44] N. R. Jones, Z. U. Qureshi, R. J. Temple, *et al.*, "Two metres or one: what is the evidence for physical distancing in COVID-19?," *BMJ*, vol. 370, p. Article ID m3223, 2020.
https://doi.org/10.1136/bmj.m3223.

[45] K. A. Prather, C. C. Wang, and R. T. Schooley, "Reducing transmission of SARS-CoV-2," *Science*, vol. 368, no. 6498, pp. 1422–1424, 2020.
https://doi.org/10.1126/science.abc6197.

[46] J. W. Tang, T. J. Liebner, B. A. Craven, and G. S. Settles, "A schlieren optical study of the human cough with and without wearing masks for aerosol infection control," *Journal of The Royal Society Interface*, vol. 6, no. suppl_6, pp. S727–S736, 2009.
https://doi.org/10.1098/rsif.2009.0295.focus.

[47] S. Asadi, C. D. Cappa, S. Barreda, *et al.*, "Efficacy of masks and face coverings in controlling outward aerosol particle emission from expiratory activities," *Scientific reports*, vol. 10, no. 1, pp. 1–13, 2020.
https://doi.org/10.1038/s41598-020-72798-7.

[48] C. J. Worby and H.-H. Chang, "Face mask use in the general population and optimal resource allocation during the COVID-19 pandemic," *Nature Communications*, vol. 11, p. 4049, Aug 2020.
https://doi.org/10.1038/s41467-020-17922-x.

[49] European Committee for Standardization, "EN 14683:2019+AC:2019, Medical face masks - Requirements and test methods," standard, CEN, Brussels, 2019.

[50] J. Pan, C. Harb, W. Leng, and L. C. Marr, "Inward and outward effectiveness of cloth masks, a surgical mask, and a face shield," *Aerosol Science and Technology*, pp. 1–16, Feb 2021.
https://doi.org/10.1080/02786826.2021.1890687.

[51] D. J. Huang and V. Huang, "Evaluation of the efficiency of medical masks and the creation of new medical masks," *Journal of International Medical Research*, vol. 35, no. 2, pp. 213–223, 2007.
https://doi.org/10.1177/147323000703500205.

[52] W. C. Adams, "Measurement of breathing rate and volume in routinely performed daily activities," tech. rep., California Air Resources Board, 1993.

[53] United States Environmental Protection Agency, *Exposure Factors Handbook 2011 Edition (Final Report), EPA/600/R-09/052F*. Washington, DC: U.S. EPA, 2011.
https://cfpub.epa.gov/ncea/risk/recordisplay.cfm?deid=236252.

[54] M. Gameiro da Silva, "Virtual laboratories for a course on indoor environmental quality," *International Journal of Online Engineering*, vol. 5, pp. 20–26, 11 2009.
https://online-journals.org/index.php/i-joe/article/view/1107.

[55] A. Litiu, "Ventilation system types in some EU countries," *Rehva Journal*, vol. 1, pp. 18–23, Jan 2012.
https://www.rehva.eu/rehva-journal/detail/01-2012.

[56] R. Daniels, "BB 101: Ventilation, thermal comfort and indoor air quality 2018," report, UK government - Education and Skills Funding Agency, London, 2018. https://www.gov.uk/government/publications/building-bulletin-101-ventilation-for-school-buildings.

[57] C. Allocca, Q. Chen, and L. R. Glicksman, "Design analysis of single-sided natural ventilation," *Energy and Buildings*, vol. 35, no. 8, pp. 785–795, 2003. https://doi.org/10.1016/S0378-7788(02)00239-6.

[58] W. Bobenhausen, *Simplified design of HVAC systems*. John Wiley & Sons, 1994.

[59] N. van Doremalen, T. Bushmaker, D. H. Morris, *et al.*, "Aerosol and surface stability of SARS-CoV-2 as compared with SARS-CoV-1," *New England Journal of Medicine*, vol. 382, no. 16, pp. 1564–1567, 2020. https://doi.org/10.1056/NEJMc2004973.

[60] J. D. Noti, F. M. Blachere, C. M. McMillen, *et al.*, "High humidity leads to loss of infectious influenza virus from simulated coughs," *PLOS ONE*, vol. 8, pp. 1–8, 02 2013. https://doi.org/10.1371/journal.pone.0057485.

[61] W. Yang, S. Elankumaran, and L. C. Marr, "Relationship between humidity and influenza a viability in droplets and implications for influenza's seasonality," *PLOS ONE*, vol. 7, pp. 1–8, 10 2012. https://doi.org/10.1371/journal.pone.0046789.

[62] A. C. Lowen, S. Mubareka, J. Steel, and P. Palese, "Influenza virus transmission is dependent on relative humidity and temperature," *PLOS Pathogens*, vol. 3, pp. 1–7, 10 2007. https://doi.org/10.1371/journal.ppat.0030151.

[63] D. H. Morris, K. C. Yinda, A. Gamble, *et al.*, "Mechanistic theory predicts the effects of temperature and humidity on inactivation of SARS-CoV-2 and other enveloped viruses," *bioRxiv*, 2020. https://doi.org/10.1101/2020.10.16.341883.

[64] J. L. Perry, J. Agui, and R. Vijayakimar, "Submicron and nanoparticulate matter removal by HEPA-rated media filters and packed beds of granular materials," *NASA/TM-2016-218224*, pp. 1–28, 2016. https://ntrs.nasa.gov/citations/20170005166.

[65] S. Miller-Leiden, C. Lohascio, W. W. Nazaroff, and J. Macher, "Effectiveness of in-room air filtration and dilution ventilation for tuberculosis infection control," *Journal of the Air & Waste Management Association*, vol. 46, no. 9, pp. 869–882, 1996. https://doi.org/10.1080/10473289.1996.10467523.

[66] European Committee for Standardization, "EN 1882:2019, High efficiency air filters (EPA, HEPA and ULPA) - Part 1: Classification, performance testing, marking," standard, CEN, Brussels, 2019.

[67] International Organization for Standardization, "ISO 14644-3:2019, Cleanrooms and associated controlled environments — Part 3: Test methods," standard, ISO, Geneva, 2019.

[68] A. Fernstrom and M. Goldblatt, "Aerobiology and its role in the transmission of infectious diseases," *Journal of Pathogens*, vol. 2013, p. Article ID 493960, Jan 2013. https://doi.org/10.1155/2013/493960.

[69] The National Institute for Occupational Safety and Health, "NIOSH-42 CFR Part 84, Respiratory Protective Devices," standard, NIOSH, Washington DC, 1995.

[70] European Committee for Standardization, "EN 149:2001+A1:2009, Respiratory protective devices - Filtering half masks to protect against particles - Requirements, testing, marking," standard, CEN, Brussels, 2009.

[71] C. M. Booth, M. Clayton, B. Crook, and J. Gawn, "Effectiveness of surgical masks against influenza bioaerosols," *Journal of Hospital Infection*, vol. 84, no. 1, pp. 22–26, 2013. https://doi.org/10.1016/j.jhin.2013.02.007.

[72] W. C. Hinds, *Aerosol technology: properties, behavior, and measurement of airborne particles*, pp. 233 – 259. New York: Wiley, 1999.

[73] W. Sungnak, N. Huang, C. Bécavin, *et al.*, "SARS-CoV-2 entry factors are highly expressed in nasal epithelial cells together with innate immune genes," *Nature medicine*, vol. 26, no. 5, pp. 681–687, 2020.
https://doi.org/10.1038/s41591-020-0868-6.

[74] B. G. Madas, P. Füri, Á. Farkas, *et al.*, "Deposition distribution of the new coronavirus (SARS-CoV-2) in the human airways upon exposure to cough-generated droplets and aerosol particles," *Scientific reports*, vol. 10, no. 1, pp. 1–8, 2020.
https://doi.org/10.1038/s41598-020-79985-6.

[75] World Health Organization, "Transmission of SARS-CoV-2: implications for infection prevention precautions: scientific brief, 09 July 2020," sci. brief, World Health Organization, Geneva, 2020. License: CC BY-NC-SA 3.0 IGO,
https://apps.who.int/iris/handle/10665/333114.

[76] C. B. Beggs, C. J. Noakes, P. A. Sleigh, and others., "The transmission of tuberculosis in confined spaces: an analytical review of alternative epidemiological models," *The International Journal of Tuberculosis and Lung Disease*, vol. 7, no. 11, pp. 1015–1026, 2003.
https://www.ingentaconnect.com/content/iuatld/ijtld/2003/00000007/00000011/art00002.

[77] A. Endo, S. Abbott, A. Kucharski, and S. Funk, "Estimating the overdispersion in COVID-19 transmission using outbreak sizes outside china," *Wellcome Open Research*, vol. 5, no. 67, 2020.
https://doi.org/10.12688/wellcomeopenres.15842.3.

[78] J. O. Lloyd-Smith, S. J. Schreiber, P. E. Kopp, and W. M. Getz, "Superspreading and the effect of individual variation on disease emergence," *Nature*, vol. 438, no. 7066, pp. 355–359, 2005.
https://doi.org/10.1038/nature04153.

[79] D. A. Edwards, D. Ausiello, J. Salzman, *et al.*, "Exhaled aerosol increases with COVID-19 infection, age, and obesity," *Proceedings of the National Academy of Sciences*, vol. 118, no. 8, p. e2021830118, 2021.
https://doi.org/10.1073/pnas.2021830118.

[80] C.-M. Liao, C.-F. Chang, and H.-M. Liang, "A probabilistic transmission dynamic model to assess indoor airborne infection risks," *Risk Analysis*, vol. 25, no. 5, pp. 1097–1107, 2005.
https://doi.org/10.1111/j.1539-6924.2005.00663.

[81] World Health Organization, United Nations Children's Fund (UNICEF), United Nations Educational, Scientific and Cultural Organization, "Considerations for school-related public health measures in the context of covid-19: annex to considerations in adjusting public health and social measures in the context of covid-19, 14 september 2020," annex, World Health Organization, 2020. License: CC BY-NC-SA 3.0 IGO,
https://apps.who.int/iris/handle/10665/334294.

[82] J. Curtius, M. Granzin, and J. Schrod, "Testing mobile air purifiers in a school classroom: Reducing the airborne transmission risk for SARS-CoV-2," *Aerosol Science and Technology*, pp. 1–14, 2021.
https://doi.org/10.1080/02786826.2021.1877257.

[83] European Centre for Disease Prevention and Control, "Heating, ventilation and air-conditioning systems in the context of COVID-19, 09 november 2020," tech. rep., ECDC, Stockholm, 2020. https://www.ecdc.europa.eu/en/publications-data/heating-ventilation-air-conditioning-systems-covid-19.

[84] A. Damialis, S. Gilles, M. Sofiev, *et al.*, "Higher airborne pollen concentrations correlated with increased sars-cov-2 infection rates, as evidenced from 31 countries across the globe," *Proceedings of the National Academy of Sciences*, vol. 118, no. 12, p. e2019034118, 2021.
https://doi.org/10.1073/pnas.2019034118.

[85] J. J. A. van Kampen, D. A. M. C. van de Vijver, P. L. A. Fraaij, B. L. Haagmans, M. M. Lamers, N. Okba, *et al.*, "Duration and key determinants of infectious virus shedding in hospitalized patients with coronavirus disease-2019 (COVID-19)," *Nature Communications*, vol. 12, p. 267, Jan 2021. https://doi.org/10.1038/s41467-020-20568-4.

[86] R. P. Rannan-Eliya, N. Wijemunige, J. R. N. A. Gunawardana, *et al.*, "Increased intensity of pcr testing reduced COVID-19 transmission within countries during the first pandemic wave," *Health Affairs*, vol. 40, no. 1, pp. 70–81, 2021. https://doi.org/10.1377/hlthaff.2020.01409.

[87] G. Pilarowski, P. Lebel, S. Sunshine, *et al.*, "Performance Characteristics of a Rapid Severe Acute Respiratory Syndrome Coronavirus 2 Antigen Detection Assay at a Public Plaza Testing Site in San Francisco," *The Journal of Infectious Diseases*, 01 2021. https://doi.org/10.1093/infdis/jiaa802.